Electronic Journal of Differential Equations, Vol. 2018 (2018), No. 106, pp. 1–34.
ISSN: 1072-6691. URL: http://ejde.math.txstate.edu or http://ejde.math.unt.edu

HEISENBERG FERROMAGNETISM AS AN EVOLUTION OF A SPHERICAL INDICATRIX: LOCALIZED SOLUTIONS AND ELLIPTIC DISPERSIONLESS REDUCTION

FRANCESCO DEMONTIS, GIOVANNI ORTENZI, MATTEO SOMMACAL

Communicated by Tuncay Aktosun

Abstract. A geometrical formulation of Heisenberg ferromagnetism as an evolution of a curve on the unit sphere in terms of intrinsic variables is provided and investigated. Given a vortex filament moving in an incompressible Euler fluid with constant density (under the local induction approximation hypotheses), the solutions of the classical Heisenberg ferromagnet equation are represented by the corresponding spherical (or tangent) indicatrix. The equations for the time evolution of the indicatrix on the unit sphere are given explicitly in terms of two intrinsic variables, the geodesic curvature and the arc-length of the curve. Notably, by considering the evolution with respect to slow variables and neglecting the dispersive terms, a novel elliptic dispersionless reduction of the Heisenberg ferromagnet model is obtained. The length of the spherical indicatrix is proved not to be conserved. Finally, a totally explicit algorithm is provided, allowing to construct a solution of the Heisenberg ferromagnet equation from a solution of Nonlinear Schrödinger equation, and, remarkably, viceversa, allowing to construct a solution of Nonlinear Schrödinger equation from a solution of the Heisenberg ferromagnet equation. As expected from the Zakharov-Takhtajan gauge equivalence, in the reflectionless case such a two-way map between solutions is shown to preserve the Inverse Scattering Transform spectra, and thus the localization.

1. Introduction

In this work we provide a geometrical formulation of Heisenberg ferromagnetism as an evolution of a curve on the unit sphere. In the present context, we refer to Heisenberg ferromagnetism as the magnetization dynamics of a continuous, isotropic ferromagnet in (1+1) dimensions (space and time). In particular, we will derive an elliptic dispersionless reduction for the evolution of the curve on the unit sphere, expressed in terms of intrinsic variables (a geodesic curvature and a quantity related to a metric on the curve), and we will carry out a systematic study of the spherical curves corresponding to localized configurations of the magnetic field. Our starting point will be the established connection [21, 37, 53] between

2010 *Mathematics Subject Classification.* 35C08, 35J62, 35Q35, 35Q51, 53C44.
Key words and phrases. Classical Heisenberg ferromagnet equation; curve motion; nonlinear Schroedinger equation; vortex filament binormal motion; dispersionless reduction; localized solution.
©2018 Texas State University.
Submitted January 17, 2018. Published May 7, 2018.

the focusing nonlinear Schrödinger equation (NLS) and the continuous, classical Heisenberg ferromagnet equation (HF) through the Da Rios model (DR).

Before explaining the geometrical link between NLS and HF, it is fundamental to introduce these two equations, along with briefly commenting on their theoretical and applied relevance within the study of nonlinear wave phenomena.

The wider physical importance of the NLS equation became evident after the works of Chiao et al [17] and Talanov [79, 80], especially in connection with the phenomena of self-focusing/self-defocusing and the conditions under which an electromagnetic beam can propagate in nonlinear media without spreading. Since then, equations of NLS-type have been derived in such diverse fields as deep water waves [4, 86], plasma physics [87], nonlinear fiber optics [35, 36], Bose-Einstein condensates [75], etc. As a matter of fact, most dispersive energy preserving systems give rise, in appropriate limits, to the scalar NLS equation, which explains the keen interest in NLS as a prototypical integrable system (see [15]).

The discovery in [86] that the initial value problem associated to the focusing/defocusing NLS equation

$$\begin{aligned} iu_t + u_{ss} + 2\varepsilon|u|^2u = 0,\\ u(s,0) = u^{(0)}(s) \end{aligned} \tag{1.1}$$

can be solved via the Inverse Scattering Transform (IST) technique led to an extensive amounts of studies, devoted to both the focusing ($\varepsilon = 1$) and the defocusing ($\varepsilon = -1$) dispersion regimes. For a detailed account of IST we refer the reader to the classical textbooks [2, 3, 4, 16, 67]. In equation (1.1), u is a function depending on the variables s and t. Subscripts s and t denote differentiation throughout. In the context of IST, the unknown function u is usually referred to as the potential. The IST method has been applied in the case of potentials $u(s,t)$ which rapidly decay as $|s| \to \infty$ [2, 3, 4, 16, 67], as well as in the case of potentials which do not decay at infinity [8, 9, 11, 12, 22, 23, 29, 32, 33, 46, 47, 50, 58]. In the present paper we focus our attention on the focusing NLS equation with vanishing potentials, for which an explicit soliton solution formula has been found in [6] by using the so-called matrix triplet method. We will briefly describe the matrix triplet method at the end of this section because it will play a fundamental role in this paper.

On the other hand, the continuous Heisenberg ferromagnet chain equation (i.e., the one-dimensional, isotropic Landau-Lifshitz equation) is the simplest and most fundamental of the continuous, integrable models of ferromagnetism, capable of accounting for the existence of localized, propagating, solitary waves of the magnetic field in a nano-wire. Recently, an increasing number of theoretical and experimental advancements have renewed the interest towards the study of localized, propagating configurations of the magnetic field in (two- and three-dimensional) ferromagnetic materials at the nanometer length-scale [57, 10]. This has always been a challenging ground, particularly because of the dimensions of the length-scale at which such nonlinear wave phenomena – denominated (non-topological) magnetic-droplet solitons – are predicted to occur (e.g., [14, 38, 39, 40, 43, 44, 45, 49, 76]). The first enucleation of a magnetic-droplet soliton in a nano-contact spin-torque oscillator device has been announced in 2013 [62], followed by further theoretical and experimental investigation (e.g., see [13, 18, 19, 20, 60, 61, 63]). Interesting dynamical features have been reported, including oscillatory motions, as well as "spinning"

and "breather" states. In particular, in [41], it has been shown how, as an extended magnetic thin film is reduced to a nano-wire with a nano-contact of fixed size at its center, the observed excited modes undergo transitions from a localized two-dimensional droplet into a pulsating one-dimensional droplet, linking the study of low-dimensional magnetic solitons to the recent experimental discoveries.

The HF equation reads

$$\mathbf{m}_t = \mathbf{m} \times \mathbf{m}_{ss}\,, \tag{1.2a}$$

where $\mathbf{m} : \mathbb{R} \times \mathbb{R} \to \mathbb{S}^2$, $\mathbf{m}(s,t) = \sum_{j=1}^{3} m_j(s,t)\mathbf{e}_j$, is the magnetization vector at position s and time t, and the vectors $\mathbf{e}_j$, $j = 1, 2, 3$, are the standard cartesian basis vectors for $\mathbb{R}^3$, and $\mathbb{S}^2$ is the sphere in $\mathbb{R}^3$ (note that $\|\mathbf{m}(x,t)\| = 1$). We assume that the position s is taken on the real line orientated as $\mathbf{e}_1$. Equation (1.2) is the well-known continuous limit of the (quantum) ferromagnetic Heisenberg chain in a constant field when the wavelength of the excited modes is larger than the lattice distance (see, for instance, [1, 30, 51]). Furthermore, we observe that in the right-hand side of (1.2) one can add a term of the form $h\mathbf{m} \times \mathbf{e}_3$ with $h \in \mathbb{R}$, which can be scaled out by a convenient change of variables (see [30, 39]).

Usually, equation (1.2) is associated to some asymptotic or initial condition. We will discuss this aspect from a geometrical point of view in Section 2; at the moment it suffices to say that a typical asymptotic condition consists in assuming that the constant spin field of the ground state of the Heisenberg chain points as $\mathbf{e}_3$, namely

$$\mathbf{m}(s,t) \to \mathbf{e}_3 \quad \text{as } s \to \pm\infty. \tag{1.2b}$$

It is well known that also (1.2) is integrable [30, 53, 81, 88] and hence it has all the properties which characterize integrable equations. The existence of localized, propagating, solitary waves was first derived in [52, 64, 82]. In [81], Takhtajan showed that (1.2) admits a Lax pair representation which assures that the IST technique (see [4, 16, 29]) can be applied to solve the HF equation (1.2) with initial-value $\mathbf{m}(s,0) = \mathbf{m}^{(0)}(s)$, see [81, 88]. In particular, the Marchenko equations and the time dependence of the scattering data are presented in [81], as well as the one-soliton solution and the phase and centre-of-mass shifts for a two-soliton collision. In [30], extending the results in [81], a diagonal action-angle representation of (1.2) is exhibited. Furthermore, using the so-called Hasimoto map [37, 54], Lakshmanan was able to prove in [53] the existence of an infinite number of constants of motion for the HF equation. In particular, in [53], employing the same geometrical connection between NLS and HF that we exploit in the present work (see also [54]), it is shown that the energy and the momentum density of the magnetization vector admit soliton solutions and their explicit expressions are given for the one soliton solution. Recently, in [24], using the matrix-triplet method, a closed-form soliton solution formula has been found for (1.2), containing all the soliton solutions of 1.2, and leading to their classification.

In [88], the existence of a gauge equivalence between (1.2) and (1.1) is established. In that work, Zakharov and Takhtajan observe that the results in [53] are (verbatim) "simple consequences of this equivalence". However, in general it is not easy to use such an equivalence to write explicitly a solution of the NLS equation from an explicit solution of the HF equation, and viceversa. On the contrary, using the matrix-triplet formulae derived in [6] and [24], we are able to exploit the geometrical connection between NLS and HF to carry out a totally explicit construction of HF reflectionless solutions from NLS reflectionless solutions and viceversa: by doing

this, we extend to the actual, explicit solutions (in both directions, from NLS to HF and from HF to NLS) the results of [53] and [56] for the conserved quantities of HF from NLS; moreover, this bi-directional construction suggests that, in the reflectionless case, the geometrical link between NLS and HF can be indeed regarded as a "geometrical implementation" of the Zakharov-Takhtajan gauge equivalence, for it preserves the IST spectrum – possibly except for a (non-trivial) rescaling of the IST norming constants – and hence the localization of the solutions.

In [65] the authors generalized this connection, by showing that a gauge equivalence exists between the NLS equation and the Landau-Lifshitz equation (LL), i.e. the model where the anisotropy is taken into account. The Hasimoto map and the geometric connection between NLS and HF has been used in [34] in the context of the study of self-similar solutions of the isotropic Landau-Lifshitz-Gilbert equation. Furthermore, it has been employed in [83] to derive a hydrodynamic counterpart for the continuous Heisenberg chain, which is alternative, but different, to the dispersionless model obtained here for the first time (to the best of our knowledge).

The key to analyze the connection between the NLS equation and Heisenberg equation is the so-called binormal equation (see equation (1.3) below). This equation allows to develop a physical insight into the link between the motion of a vortex filament in an incompressible, Eulerian fluid with constant density [21] and the evolution of the magnetic field in a one-dimensional ferromagnet as described by the continuous Heisenberg model (1.2). This connection has been established separately and independently in several works (see [37, 53, 55, 83, 88], already mentioned above), using the focusing NLS equation as *Ur-system*. The two systems involved in this connection belong to the two rather different physical domains of hydrodynamics and ferromagnetism.

The motion of a vortex filament in an incompressible, Eulerian fluid with constant density is a classical problem which is still unsolved for generic initial conditions. One of the most important models allowing to achieve an approximate solution of this initial value problem exploits the so-called Local Induction Approximation (LIA) [77]. The main hypotheses on this approximation are as follows: (1) the section of the vortex core is negligible, and, (2) the self-interaction of the filament is local. Under the LIA approximation the vortex filament is described by a curve $\mathbf{X} = \mathbf{X}(s,t) \in \mathbb{R}^3$ parameterized by the arc-length s and evolving in time t. Let $(\mathbf{t}, \mathbf{n}, \mathbf{b})$ be the standard Frenet-Serret frame along the vortex filament curve $\mathbf{X}$, with $\mathbf{t}$ being the unit tangent vector, $\mathbf{n}$ the unit normal vector, and $\mathbf{b}$ the unit normal vector. Then, it is well known [77] that, in this context, the vortex motion is described by the following binormal equation

$$\mathbf{X}_t = \mathbf{X}_s \times \mathbf{X}_{ss} \equiv \tilde{\kappa}\mathbf{b}\,. \tag{1.3}$$

Hasimoto in [37] has shown that the curvature and the (derivative of the) torsion corresponding to this curve are connected respectively to the amplitude and the phase of a solution of the focusing NLS equation via the so-called Hasimoto map. In this sense equation (1.3) is integrable. The binormal motion of a vortex filament, under the LIA and other approximations, has been extensively studied in [70, 71, 72, 73, 74], along with the integrable connection that it provides between NLS and HF, as well as generalizations of these two equations.

The diagram 1 shows the strategy that we follow to achieve our result. We will briefly discuss the diagram later in this Section and, in a more detailed way, in Section 2. Let us remark that the horizontal arrow between the binormal curve

and curve on the sphere represents the counterpart in the case of curve motions of the gauge transformation introduced in [88].

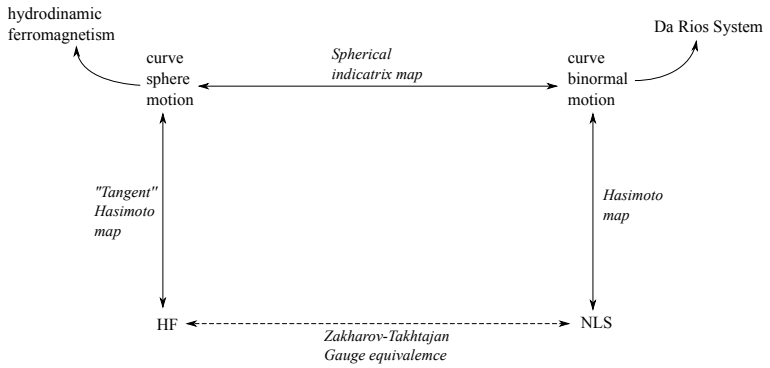

Figure 1: Diagram of the connections between Heisenberg ferromagnetism, focusing NLS equation and their curve motions-hydrodynamics counterparts.

Indeed, if we focus our attention on equation (1.3), we can introduce a map, denoted from now on by $\mathcal{B}$, connecting the binormal motion on the curve $\mathbf{X}(s,t)$ and the "geometric" curve γ on the sphere (the curve γ is the geometric interpretation of the vector of the magnetization $\mathbf{m}(s,t)$). In particular, if we denote by $\tilde{\kappa}$, $\tilde{\tau}$ the curvature and the torsion, respectively, of the curve $\mathbf{X}(s,t)$, and by κ, τ the curvature and the torsion, respectively, of the curve γ, then it turns out that the map $\mathcal{B}$ is "almost" invertible (in the sense explained below) and we will prove that:

(1) If a soliton solution of the NLS equation is given, first we can construct $\tilde{\kappa}$, $\tilde{\tau}$ via the Hasimoto map, and then we get κ, τ via the map $\mathcal{B}$, thereby obtaining the curvature and the torsion corresponding to a specific solution of the HF equation. For the sake of clarity, we remind here that it is well-known that a curve is uniquely determined up to Euclidean movements once its (non-zero) curvature and torsion are (globally) assigned (see any standard textbook in geometry: for instance, [85]).

(2) Starting from a soliton solution of the HF equation such that the curvature, κ, and the torsion, τ, of the curve γ on the sphere are the same ones obtained in the preceding step (1), then, by inverting the map $\mathcal{B}$, one finds exactly the curvature, $\tilde{\kappa}$, and the torsion, $\tilde{\tau}$, for the vortex filament as obtained in the previous step (1) via the Hasimoto map.

The map $\mathcal{B}$ allows to link the purely geometric binormal motion with a curve motion on the sphere, and this fact can be seen as an interesting characterization for the binormal motion.

Moreover it turns out (see Section 2) that, instead of κ and τ, some features of the curve motion on the sphere are better described in terms of two intrinsic variables, the geodesic curvature K, and $v = \sigma_s$ which represents the derivative of the arc-length of the curve on the sphere σ with respect to the arc-length s of the binormal curve $\mathbf{X}(s,t)$. In particular, such variables allows to introduce an elliptic dispersionless reduced model for the evolution of the curve on the unit sphere (see formula (2.26) in Section 2), resemblant of the elliptic dispersionless reduction of

the focussing NLS equation (see [28]), and alternative to the dispersionless models for the Heisenberg equation already known in the literature, which focus mainly on the hyperbolic case (e.g., see [78, 69, 42], as well as [83], where the geometric connection with NLS is also – but differently – employed). The analysis of this new elliptic dispersionless model will be the subject of future investigation.

It is rather remarkable that the new variables K and σ_s can be used to establish an explicit formula connecting the curvature and the torsion on the sphere to the magnetization vector $\mathbf{m}(s,t)$. Moreover, as we have already pointed out, the connection can be used to show how to produce an explicit soliton solution formula for the NLS equation if an explicit soliton solution of the HF equation is given (in fact it is "enough" to follow the solid arrows from HF to NLS in the diagram). Unfortunately, the solid lines from NLS to HF in the diagram cannot be followed easily because of the difficulties in producing explicitly the magnetization vector if κ and τ are given. To overcome these difficulties we have implemented a numerical approach to get a solution of the HF equation when a soliton solution of the NLS is given. To reach this result, starting from a solution of NLS, we construct $\tilde{\kappa}$ and $\tilde{\tau}$ by means of the Hasimoto map; then we integrate numerically the Frenet-Serret system

$$\frac{d}{ds}\begin{pmatrix}\mathbf{t}\\ \mathbf{n}\\ \mathbf{b}\end{pmatrix} = \begin{pmatrix}0 & \tilde{\kappa} & 0\\ -\tilde{\kappa} & 0 & \tilde{\tau}\\ 0 & -\tilde{\tau} & 0\end{pmatrix}\begin{pmatrix}\mathbf{t}\\ \mathbf{n}\\ \mathbf{b}\end{pmatrix}, \tag{1.4}$$

with an initial condition satisfying the boundary condition $\mathbf{t}(\pm\infty,0)\to e_3$ and the orthogonality of the (unknown) Frenet-Serret frame. It turns out (see Section 2) that the tangent vector $\mathbf{t}(s,t)$ coincides with the magnetization vector $\mathbf{m}(s,t)$. By integrating the Frenet-Serret system (1.4) at $t=0$, we get numerically the initial condition $\mathbf{m}(s,0)$. We can use this latter initial condition to solve numerically the initial value problem for the Heisenberg equation (1.2) with $\mathbf{m}(s,0)=\mathbf{m}^{(0)}(s)$ by means of the method of lines with a pseudospectral, Fourier discretization in space and an adaptive Runge-Kutta scheme in time.

Finally, the solution of the HF equation obtained numerically by means of the above procedure, starting from an explicit, reflectionless solution of the NLS equation for a certain choice of the NLS spectral data, has been compared to the explicit solution of the HF equation obtained from the same spectral data: as expected, in all cases we found a perfect correspondence.

We use both the reflectionless solution formula for the NLS equation [6] and the reflectionless solutions of the HF equation [24], as they emerge from the application of the matrix triplet method. Thus, it is important to briefly describe this method, applied in [6] to solve the scalar NLS equation, and then proved successful in solving several other integrable partial differential equations (see, for instance, [5, 7, 24, 25, 26]). It is well known [86, 4] that to get the solution of a given integrable evolutionary equation for which the IST can be applied, it is necessary to develop the inverse scattering theory for a suitable, associated scattering problem. The so-called matrix triplet method can be successfully used whenever the inverse scattering theory can be formulated in terms of integral Marchenko equations. The main idea of the method is to represent the kernel of the Marchenko equation as $Ce^{(y+z)A}B$, where (A,B,C) is a "suitable" matrix triplet containing the scattering data, i.e., the spectrum of the scattering problem. The particular representation of the kernel of the Marchenko equation allows to solve the Marchenko equations

explicitly, and then to get closed-form solutions of the integrable equation to which it is applied. The solutions obtained in this way will not contain anything more complicated than matrix exponentials and solutions of matrix Lyapunov equations, and, if necessary, can hence be "unzipped" into (lengthy) expressions containing elementary functions, or used as input for numerical calculations.

This paper is organized as follows. In Section 2 a geometrical formulation of Heisenberg ferromagnetism as an evolution of a curve on the unit sphere γ in terms of intrinsic variables is provided. In particular, by using as intrinsic variables the geodesic curvature K of the curve γ on the unit sphere and the derivative of the arc-length of γ with respect to the arc-length along the Da Rios curve, we obtain that the evolution of the Heisenberg curve γ is described by a PDE system possessing an elliptic dispersionless reduction. In Section 3 we show how to explicitly connect a solution of the HF equation to a solution of the NLS equation and viceversa. The procedure is explained in the case of arbitrary reflectionless potentials, proving the presevation of the localization under action of the spherical indicatrix map $\mathcal{B}$. Finally, in Appendix 5, starting from the matrix-triplet formulae from (3.18) and (3.19), we derive alternative expressions of the reflectionless solutions of NLS and HF (and of their time- and space-derivatives), respectively, which are more convenient for their numerical evaluation.

2. Vortex binormal motion vs Heisenberg equation

In this Section we focus on the possible geometric motions associated to the focusing NLS equation, that is

$$iu_t + u_{ss} + 2|u|^2 u = 0\,, \tag{2.1}$$

by analyzing the connections between it, the Da Rios (see equation (2.4) below) and the Heisenberg equations (1.2).

As mentioned in the Introduction, the first connection between the focusing NLS equation and the motion of a Euler vortex filament in the so called local induction approximation [77] has been made by Hasimoto in [37]. The vortex filament – which is described by a curve $\mathbf{X} = \mathbf{X}(s,t) \in \mathbb{R}^3$ parameterized by the arc-length s – evolves in time t by following the binormal equation

$$\mathbf{X}_t = \mathbf{X}_s \times \mathbf{X}_{ss} \equiv \tilde{\kappa}\,\mathbf{b}\,,$$

where $\mathbf{b}$ is the binormal unit vector [77]. Hasimoto introduced a map connecting the curvature $\tilde{\kappa}$ and torsion $\tilde{\tau}$ of the vortex filament with the amplitude and phase of the NLS solution u of (2.1) as follows:

$$u = \frac{\tilde{\kappa}}{2} e^{\int \tilde{\tau}\mathrm{ds}} \tag{2.2}$$

In particular, equation (2.2) implies

$$\tilde{\kappa} = 2|u|\,, \quad \tilde{\tau} = \theta_s = \frac{1}{2i}\Big(\frac{u_s}{u} - \frac{u_s^*}{u^*}\Big). \tag{2.3}$$

Explicitly, we obtain the well known Da Rios system [21],

$$\tilde{\kappa}_t + 2\tilde{\tau}\tilde{\kappa}_s + \tilde{\tau}_s\tilde{\kappa} = 0\,, \quad \tilde{\tau}_t + \Big(\tilde{\tau}^2 - \frac{1}{2}\tilde{\kappa}^2 - \frac{\tilde{\kappa}_{ss}}{\tilde{\kappa}}\Big)_s = 0\,. \tag{2.4}$$

The binormal equation (1.3), and, consequently the focusing NLS equation, is related in a geometric way [53] to the Heisenberg equation (1.2) (reported below for

the sake of clearness)

$$\mathbf{m}_t = \mathbf{m} \times \mathbf{m}_{ss}\,, \quad \mathbf{m} \in \mathbb{S}^2\,.$$

In fact, it is simple to observe that the Heisenberg solution $\mathbf{m}$ is the unitary tangent vector of a solution of the binormal velocity motion (1.3),

$$\mathbf{X}_s = \mathbf{m} = \mathbf{t}\,, \tag{2.5}$$

where $\mathbf{t}$ is the unit tangent vector to the vortex filament curve. Equation (2.5) allows us to interpret the solutions of the Heisenberg equations as curves on $\mathbb{S}^2$ generated by the tangent vectors of a curve in $\mathbb{R}^3$ associated to a solution of the Da Rios model [53] (see figure 2).

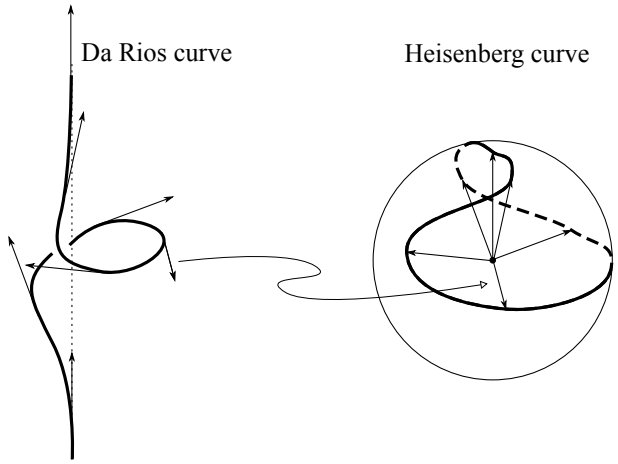

Figure 2: Example of the construction of the tangent indicatrix (right) from a curve (left). If the curve related to a Da Rios solution has the same asymptotic behavior at $s \to \pm\infty$ then the curve related to the Heisenberg solution is closed.

This is a classical geometrical construction which is called "tangent indicatrix" (e.g., see [85]). We observe that for the solutions of the Da Rios equation having the same asymptotic straight line when $s \to +\infty$ and when $s \to -\infty$ (which is always the case if the potential $u(x,t)$ of the NLS equation vanishes as $x \to \pm\infty$ for fixed t), then the associated Heisenberg solution is a closed curve on $\mathbb{S}^2$. We want to exploit such geometric relation in order to show explicitly some interesting analytical property of the Heisenberg equation. It is well known [85] that the curvature $\tilde{\kappa}$ and the torsion $\tilde{\tau}$ of the vortex filament are related to the curvature κ and the torsion τ of the tangent indicatrix associated to a Heisenberg solution curve on the sphere as follows:

$$\kappa = \sqrt{1 + \frac{\tilde{\tau}^2}{\tilde{\kappa}^2}}\,, \quad \tau = \frac{\tilde{\kappa}\tilde{\tau}_s - \tilde{\kappa}_s\tilde{\tau}}{\tilde{\kappa}(\tilde{\kappa}^2 + \tilde{\tau}^2)}\,. \tag{2.6}$$

Obviously, since the tangent indicatrix is a spherical curve by construction, κ and τ have to satisfy the relation (e.g., see [85]),

$$R^2 = \kappa^{-2} + \tau^{-2}\left[(\kappa^{-1})_\sigma\right]^2\,, \tag{2.7}$$

where $R = 1$ is the radius of the sphere, and σ is the arc-length of the curve on the sphere. We underline that, in the Da Rios equation, s denotes the arc-length of the vortex filament, and it does not coincide with the arc-length σ of the tangent indicatrix, namely of the Heisenberg solution curve on the sphere $\mathbb{S}^2$. Indeed, we have

$$\sigma(s) = \int_{-\infty}^{s} |\mathbf{m}_z(z)| \mathrm{d}\, z = \int_{-\infty}^{s} |\mathbf{X}_{zz}(z)| \, \mathrm{d}\, z = \int_{-\infty}^{s} \tilde{\kappa}(z) \, \mathrm{d}\, z \,. \tag{2.8}$$

From equation (2.7) we obtain the torsion of the spherical indicatrix:

$$\tau = \frac{\kappa_\sigma}{\sqrt{\kappa^4 - \kappa^2}} \,. \tag{2.9}$$

For the sake of clarity let us recall here that we are denoting by $\mathbf{m}$ the unit vector tangent $\mathbf{t}$ to the vortex filament, i.e., the curve in $\mathbb{R}^3$. Let $(\mathbf{T}, \mathbf{N}, \mathbf{B})$ be the Frenet frame of the Heisenberg curve γ on $\mathbb{S}^2$, i.e., the curve representing the Heisenberg solution, consisting of the unit tangent vector $\mathbf{T}$, the normal vector $\mathbf{N}$, and the binormal vector $\mathbf{B}$ where

$$\mathbf{m}_\sigma = \mathbf{T} \,, \quad \kappa \mathbf{N} = \mathbf{T}_\sigma \,, \quad \mathbf{B} = \mathbf{T} \times \mathbf{N} \,. \tag{2.10}$$

It is natural to use the intrinsic notion of geodesic curvature K of a curve on the unit sphere defined as (see [85] for more details)

$$\kappa \mathbf{N} = K \hat{\mathbf{N}} - \mathbf{m} \,, \tag{2.11a}$$

where the vector $\hat{\mathbf{N}}$ is the so-called tangent normal vector ,

$$\hat{\mathbf{N}} = \mathbf{m} \times \mathbf{T} \,, \tag{2.11b}$$

satisfying the relation

$$\hat{\mathbf{N}}_\sigma = -K \mathbf{T}. \tag{2.11c}$$

Then, from (2.11a), we have

$$K \equiv \sqrt{\kappa^2 - 1} = \frac{|\tilde{\tau}|}{\tilde{\kappa}} \,, \tag{2.12}$$

and, from (2.9) and (2.12), we get

$$\tau = \frac{K_\sigma}{1 + K^2} = [\arctan(K)]_\sigma \,. \tag{2.13}$$

The relations (2.12) and (2.13) show that a spherical curve $\mathbf{m}$ can be reconstructed starting only from its geodesic curvature in the same manner as a curve in a plane can be constructed only from its curvature. This fact can be also seen by using the Taylor development in $\bar{\sigma} = \sigma - \sigma_0$,

$$\mathbf{m} = \mathbf{m}(\sigma_0) + \mathbf{m}_\sigma(\sigma_0) \, \bar{\sigma} + \frac{1}{2} \mathbf{m}_{\sigma\sigma}(\sigma_0) \, \bar{\sigma}^2 + \frac{1}{6} \mathbf{m}_{\sigma\sigma\sigma}(\sigma_0) \, \bar{\sigma}^3 + \dots \tag{2.14}$$

By using the Frenet frame of the curve on $\mathbb{S}^2$, we can reconstruct the curve from K as

$$\begin{aligned} \mathbf{m} =& \mathbf{m}(\sigma_0) + \Big(\bar{\sigma} - \frac{(1 + K^2)}{6} \, \bar{\sigma}^3 + \dots \Big) \mathbf{T} + \Big(\frac{\sqrt{1 + K^2}}{2} \, \bar{\sigma}^2 + \frac{K K_\sigma}{6\sqrt{1 + K^2}} \, \bar{\sigma}^3 + \dots \Big) \mathbf{N} \\ &+ \Big(\frac{K_\sigma}{6\sqrt{1 + K^2}} \, \bar{\sigma}^3 + \dots \Big) \mathbf{B} \,, \end{aligned} \tag{2.15}$$

for any derivative of $\mathbf{m}$ depends only on K. Taking into account equations (2.10) and (2.11c), we see that the curve can be reconstructed by solving the following second order ODE

$$\begin{aligned} \mathbf{m}_{\sigma\sigma} &= -\mathbf{m} + K\mathbf{m}\times\mathbf{m}_\sigma\,, \\ \mathbf{m}(0) &= \mathbf{m}^{(0)}\,, \quad \mathbf{m}_\sigma(0) = \mathbf{m}_\sigma^{(0)}\,. \end{aligned} \tag{2.16}$$

The initial value problem (2.16) suggests to characterize the curve on the sphere by means of the geodesic curvature K and the arc-length σ instead of κ and τ. Before studying the curve representing the Heisenberg solution on $\mathbb{S}^2$ by choosing K and σ, let us remark two relevant features of the evolution equations for the curvature κ and the torsion τ.

(1) The variables κ and τ are particularly useful when one wants to map NLS solutions into Heisenberg ones. Indeed, by composing (2.6) and (2.3) one obtain the map

$$\kappa = \sqrt{1-\frac{(u_s\,u^* - u\,u_s^*)^2}{16\,u^3\,u^{*3}}}\,, \quad \tau = i\Big(\frac{u_s}{u}-\frac{u_s^*}{u^*}\Big)^{-1}\Big[\log\Big(1-\frac{(u_s\,u^*-u\,u_s^*)^2}{16\,u^3\,u^{*3}}\Big)\Big]_s\,. \tag{2.17}$$

(2) The structure of the evolution equations for the curvature κ and the torsion τ of the spherical curve associated to the Heisenberg solution is qualitatively different from the Da Rios system (2.4) satisfied by the curvature $\tilde\kappa$ and the torsion $\tilde\tau$. Indeed, the Da Rios system allows to easily identify a dispersionless counterpart of the model (e.g., see [48]). If the curvature κ and the torsion τ of the spherical curve associated to the Heisenberg flow are used, then a different type of structure is obtained. This is due to the differential nature of the relations (2.6) linking $\tilde\kappa$ and $\tilde\tau$ to κ and τ. In particular, after a straightforward and long computation, we find that the structure of the Heisenberg flow can be written, for the curvature κ, as follows:

$$\kappa_t = \mathcal{A}_1(\kappa,\tau)\,\kappa_{ss} + \mathcal{A}_2(\kappa,\tau)\,\kappa_s\tau_s + \mathcal{A}_3(\kappa,\tau)\tau_{ss} + \text{higher derivatives} \tag{2.18}$$

where $\mathcal{A}_1$, $\mathcal{A}_2$, and $\mathcal{A}_3$ are suitable functions whose explicit structure is not relevant. We note that an analogous formula holds for the evolution of the torsion τ. Therefore, contrarily to the Da Rios system, the curvature and torsion of the Heisenberg curves do not show a natural dispersionless quasilinear counterpart. This strange behavior is related to the lack of geometric meaning of s in the Heisenberg case.

Before describing the curve on the sphere by using the geodesic curvature K and the arc-length σ, we observe that the arc-length σ depends on the time t [21],

$$\sigma_t = \int_{-\infty}^{s}\tilde\kappa_t\,\mathrm{d}s = \int_{-\infty}^{s}(-2\tilde\tau\tilde\kappa_s - \tilde\tau_s\tilde\kappa)\,\mathrm{d}s\,, \tag{2.19}$$

whereas the arc-length s used to describe the vortex filament in $\mathbb{R}^3$ is time independent. This property is very important because, from equation (2.19), it follows that the total length of the Heisenberg curve is not conserved. Indeed, we have

$$\mathcal{L}(t) = \sigma(+\infty,t) = \int_{-\infty}^{+\infty}\tilde\kappa(s,t)\,\mathrm{d}s = 2\int_{-\infty}^{+\infty}|u(s,t)|\,\mathrm{d}s\,, \tag{2.20}$$

and, taking into account that $\tilde\kappa$ is a non-conserved density for the Da Rios evolution, it follows that also the total length of the Heisenberg curve is not conserved. In fact, integrating by parts (2.19) and taking into account that $\tilde\kappa$ vanishes at $s=\pm\infty$, we

get

$$\frac{\mathrm{d}\mathcal{L}(t)}{\mathrm{d}t} = -\int_{-\infty}^{+\infty} \tilde{\kappa}_s \tilde{\tau}\, \mathrm{d}s\,. \tag{2.21}$$

Now we are ready to write the motion of a curve on the sphere following the Heisenberg model as an intrinsic motion on the sphere by choosing the geodesic curvature K and the arc-length σ. After straightforward and long computations, we obtain

$$\mathbf{m}_t = -K{\sigma_s}^2\,\mathbf{T} + \sigma_{ss}\,\hat{\mathbf{N}}\,, \tag{2.22}$$

where $\mathbf{T} = \mathbf{m}_\sigma$ is the tangent to the curve and $\hat{\mathbf{N}}$ is the tangent normal (2.11b). The tangent component of this motion does not affect the curve motion being simply a translation along the curve itself. From(2.22) it appears that the Heisenberg equation can be interpreted as an intrinsic motion of a point moving on a spherical curve even if, as expected, the arc-length parameter is not a good parameter to express the time evolution. Actually the evolution depends explicitly also on the arc-length parameter σ as a function of a parameter s independent from t; this also implies that the evolution of the curve is not local, as it depends also on the curve length. As a consequence, this type of motion does not belong to the local motions studied, for instance, in [66], where the definition of locality requires a curve motion to be local if the coefficient of the evolution equation (in our case (2.22)) depends only on the curvature (and the torsion, if we are in $\mathbb{R}^3$). We remark that the motion of the point moving on the sphere $\mathbb{S}^2$ depends also on how the arc-length σ evolves in time.

A different way to write the motion of the Heisenberg curve is obtained by using the geodesic curvature K and the arc-length σ (in particular, by introducing (2.8) and (2.12) in (2.4)) as follows:

$$\begin{gathered} K_t = -KK_s\sigma_s + \Big(1 + K^2 - \frac{\sigma_{sss}}{{\sigma_s}^3}\Big)\sigma_{ss} + \frac{\sigma_{ssss}}{{\sigma_s}^2}\,, \\ \sigma_{st} = -{\sigma_s}^2 K_s - 3K\sigma_s\sigma_{ss}\,. \end{gathered} \tag{2.23}$$

where

$$\sigma_s \equiv \|\mathbf{m}_s\| = \|\mathbf{m}\times\mathbf{m}_s\|\,, \tag{2.24a}$$

and, by inverting (2.16),

$$K = \|\mathbf{m} + \mathbf{m}_{\sigma\sigma}\|\,. \tag{2.24b}$$

System (2.23) can be written in evolutionary form by using the geodesic curvature K (2.24b) and $\sigma_s \equiv v$ (2.24a), considered as independent variables. If we do that, we get

$$\begin{gathered} K_t = -KK_s v + \Big(1 + K^2 - \frac{v_{ss}}{v^3}\Big)\, v_s + \frac{v_{sss}}{v^2}\,, \\ v_t = -v^2 K_s - 3Kvv_s\,. \end{gathered} \tag{2.25}$$

The use of a variable v in the context of curve motions whose arc-length is time-dependent has been suggested separately in [31] in the context of planar curve shortening flows (see Lemma 3.1.1 in [31]), as well as in [66], where its square, called g, is identified with "a metric on the curve".

Putting $t = \epsilon y$, $s = \epsilon x$ and neglecting higher-order terms in ϵ we can now define the dispersionless Heisenberg model as the elliptic quasilinear system

$$\begin{gathered} K_y = -vK\,K_x + \big(1 + K^2\big)\,v_x\,, \\ v_y = -v^2\,K_x - 3Kv\,v_x\,, \end{gathered} \tag{2.26}$$

which is obtained from (2.25) without the dispersive part involving only v. This implies that the dispersionless model imposes restrictions on the local variation of the curve metric v^2: equivalently, this entails that the module $|\mathbf{m}_s|$ cannot change rapidly as a function of x.

We remark that the system (2.26) is exactly the system (2.4) by using the more convenient variables

$$v = \tilde{\kappa}\,, \quad K^2 = \frac{\tilde{\tau}^2}{\tilde{\kappa}^2}\,. \tag{2.27}$$

This mapping is not one-to-one because it requires an initial choice on the torsion sign.

An elliptic dispersionless reduction analogous to (2.26) has been studied for the focussing NLS equation (also known as Airy model) in [28] where a complete characterization of the "gradient catastrophe" for this non-hyperbolic case has been obtained. The focussing dispersionless NLS model, as shown in [83, equations (3.1) and (3.2)], can be interpreted as a particular dispersionless reduction for the Heisenberg ferromagnet equation. However, the intrinsic variables used in (2.26) have the peculiarity of providing a geometrical description of the spherical indicatrix curve whose motion is naturally associated to the Heisenberg model (1.2), and in general the choice of the more convenient variables to be used in a reduction is dictated by and depends on the physical interpretation of the solutions that one has in mind. Finally, it is worth recalling here that other hydrodynamical-like models for ferromagnetism have been proposed and studied in more-than-one dimensions (see, for instance, the early works [69] and [78]). More recently, in [42] an interesting formulation of the magnetization dynamics in a ferromagnetic thin film has also stressed the possible existence of elliptic and hyperbolic regimes, by introducing a suitable definition of a ferromagnetic analogue of the hydrodynamic "sonic line" (i.e., a parabolic line in a ferromagnetic context).

A complete study of the near-catastrophe behavior of the elliptic dispersionless Heisenberg model, as well as of the relation between (2.26) and the above-mentioned dispersionless reductions is currently under investigation and will be the subject of a future work.

3. From NLS to HF and back

In the present section we show how to explicitly connect a solution of the HF equation to a solution of the NLS equation, and viceversa. We illustrate the general procedure, providing one explicit example, the one-soliton solution; then we specialize the theory to the arbitrary reflectionless case, proving the presevation of the localization under action of the spherical indicatrix map $\mathcal{B}$.

As explained in the previous Section 2, given the magnetization $\mathbf{m}(s,t)$ with $\|\mathbf{m}\| = 1$, we can interpret it as a curve on the unit sphere $\mathbb{S}^2$ with curvature κ and torsion τ given by

$$\kappa = \frac{\|\mathbf{m}_s \times \mathbf{m}_{ss}\|}{\|\mathbf{m}_s\|^3}\,, \quad \tau = \frac{(\mathbf{m}_s \times \mathbf{m}_{ss}\,,\, \mathbf{m}_{sss})}{\|\mathbf{m}_s \times \mathbf{m}_{ss}\|^2}\,, \tag{3.1a}$$

so that

$$\kappa^2 = 1 + \frac{(\mathbf{m}_s, \mathbf{m}_t)^2}{\|\mathbf{m}_s\|^6}\,, \quad \tau = \frac{1}{\|\mathbf{m}_s\|^2}\frac{\kappa_s}{\kappa\sqrt{\kappa^2-1}} = \frac{\|\mathbf{m}_s\|}{(\mathbf{m}_s, \mathbf{m}_t)}\frac{\kappa_s}{\kappa}\,. \tag{3.1b}$$

In turn, as we have already observed in the previous sections, the Heisenberg curve on the sphere can be interpreted as the spherical indicatrix of the tangent of the Da Rios curve with curvature $\tilde{\kappa}$ and torsion $\tilde{\tau}$. Using the relations given by equations (2.6) and their inverses, namely

$$\tilde{\kappa} = \frac{\kappa_s}{\kappa\tau\sqrt{\kappa^2 - 1}}\,, \quad \tilde{\tau} = \frac{\kappa_s}{\kappa\tau}\,, \tag{3.2}$$

we obtain an explicit expression for $\tilde{\kappa}$ and $\tilde{\tau}$ in terms of the magnetization $\mathbf{m}$, which, combined with (2.3), provides an explicit connection between the solutions of HF and the solutions of NLS:

$$\tilde{\kappa} = \|\mathbf{m}_s\| = 2|u| \quad \text{and} \quad \tilde{\tau} = -\frac{(\mathbf{m}_s, \mathbf{m}_t)}{\|\mathbf{m}_s\|^2} = \operatorname{Im}\big(\frac{u_s}{u}\big)\,. \tag{3.3}$$

Then, using the Hasimoto map (2.2), we can reconstruct a solution $u(s,t)$ of NLS from $\tilde{\kappa}$ and $\tilde{\tau}$:

$$u(s,t) = \frac{\tilde{\kappa}(s,t)}{2} e^{i\int_{s_0}^{s} \tilde{\tau}(z,t)\mathrm{d}z + i\phi(t)} = \frac{\tilde{\kappa}(s,t)}{2} e^{i\Phi(s,t)}\,, \tag{3.4a}$$

where, using the Da Rios equations (2.4), we have

$$\int_{s_0}^{s} \tilde{\tau}_t(z,t)\mathrm{d}z + \frac{\mathrm{d}\phi}{\mathrm{d}t} = \frac{\tilde{\kappa}^2(s,t)}{2} - \tilde{\tau}^2(s,t) + \frac{\tilde{\kappa}_{ss}(s,t)}{\tilde{\kappa}(s,t)}\,, \tag{3.4b}$$

$$\begin{aligned} \phi(t) = &- \int_{s_0}^{s} \Big(\tilde{\tau}(z,t) - \tilde{\tau}(z,t_0)\Big)\mathrm{d}z \\ &+ \int_{t_0}^{t} \Big(\frac{\tilde{\kappa}^2(s,\eta)}{2} - \tilde{\tau}^2(s,\eta) + \frac{\tilde{\kappa}_{ss}(s,\eta)}{\tilde{\kappa}(s,\eta)}\Big)d\eta\,, \end{aligned} \tag{3.4c}$$

$$\begin{aligned} \Phi(s,t) &= \int_{s_0}^{s} \tilde{\tau}(z,t)\mathrm{d}\xi + \phi(t) \\ &= \int_{s_0}^{s} \tilde{\tau}(z,t_0)\mathrm{d}z + \int_{t_0}^{t} \Big(\frac{\tilde{\kappa}^2(s,\eta)}{2} - \tilde{\tau}^2(s,\eta) + \frac{\tilde{\kappa}_{ss}(s,\eta)}{\tilde{\kappa}(s,\eta)}\Big)\mathrm{d}\eta\,. \end{aligned} \tag{3.4d}$$

To do the opposite, given a vanishing solution $u(s,t)$ of NLS, we specialize it at $t = 0$, $u(s,0)$, and we extract the curvature $\tilde{\kappa}(s,0)$ and the torsion $\tilde{\tau}(s,0)$ via the Hasimoto map (3.3). Then we integrate numerically the Frenet-Serret system (1.4) by means of an adaptive Runge-Kutte method, over a finite interval of the arc-length s, with a choice of the initial condition such that $\mathbf{t}(\pm\infty, 0) = \mathbf{e}_3$. As explained in Section 3.2, this is always possible, provided that the curvature $\tilde{\kappa}$ is almost zero at the endpoints of the integration interval. The tangent vector $\mathbf{t}(s,0)$ obtained from the numerical integration can be seen as the initial condition $\mathbf{m}(s,0)$ to be used for integrating numerically the Heisenberg equation. This latter operation is then performed by means of a pseudo-spectral method in space and an adaptive Runge-Kutta scheme in time.

As we will show in the next Section 3.1, the case of the one-soliton solution can be carried out analytically without resorting to numerical integration, extending the construction of the conserved quantities of HF starting from a multi-soliton solution of NLS as in [53]. A complete study of conserved quantities for the Da Rios model using the map with focusing NLS equation has been performed in [56]. In the general reflectionless case, in Section 3.2 we will prove that the spherical indicatrix map $\mathcal{B}$ indeed preserves the spectrum and the localization between NLS and HF, as expected based on [88].

3.1. **An explicit example: the one-soliton solution.** We are now ready to illustrate the general setup presented above in the case of a one-soliton solution, that is, we show here how to connect explicitly a one-soliton solution of to HF equation to a one-soliton of the NLS equation and viceversa, using the spherical indicatrix map $\mathcal{B}$.

Let $a = p + i\,q \in \mathbb{B}$ be an arbitrary complex number with $p > 0$: in the context of the IST setup, the quantity ia is the spectral parameter used to construct the solution, usually referred to as the discrete eigenvalue. The three components, m_1, m_2, and m_3, of the magnetization $\mathbf{m}$ for the one-soliton solution of HF read [24]:

$$\begin{pmatrix} m_1(s,t) \\ m_2(s,t) \end{pmatrix} = \frac{1 - m_3(s,t)}{p} \begin{pmatrix} \cos\beta(s,t) & -\sin\beta(s,t) \\ \sin\beta(s,t) & \cos\beta(s,t) \end{pmatrix} \begin{pmatrix} q\cosh\alpha(s,t) \\ p\sinh\alpha(s,t) \end{pmatrix}, \tag{3.5a}$$

$$m_3(s,t) = 1 - \frac{2\,p^2}{p^2+q^2}\operatorname{sech}^2\alpha(s,t)\,, \tag{3.5b}$$

where

$$V = 4q\,, \quad \omega = 4(p^2+q^2)\,, \tag{3.5c}$$

$$\alpha(s,t) = 2\,p(s - V\,t - s_0)\,, \quad \beta(s,t) = \omega t + \frac{V}{2}(s - Vt - s_0) + \varphi_0\,, \tag{3.5d}$$

and s_0 and φ_0 are some arbitrary real numbers. Using (3.3), we can explicitly compute

$$\tilde\kappa = 4p\operatorname{sech}\left(2p(4qt - s + s_0)\right), \quad \text{and} \quad \tilde\tau = 2q\,. \tag{3.6}$$

Consequently, using (3.4d), we have

$$\Phi(s,t) = \left(4p^2 - 4q^2\right)t - 4p^2t_0 + 4q^2t_0 + 2qx - 2qx_0\,. \tag{3.7}$$

As t_0 is arbitrary at this stage, we can choose it so that $-4(p^2-q^2)t_0 - 2qx_0 = \tilde\phi_0$ (provided $q \neq \pm p$) for some real number $\tilde\phi_0$:

$$\Phi(s,t) = \left(4p^2 - 4q^2\right)t + 2qx + \tilde\phi_0\,. \tag{3.8}$$

Using (3.4a), we are now capable of constructing the solution of NLS, which corresponds – modulo a shift of the phase – to the same one-soliton solution that we would have obtained had we started from the same discrete eigenvalue ia:

$$u(s,t) = 2pe^{i(4p^2t + 2q(-2qt+s) + \tilde\phi_0)}\operatorname{sech}\left(2p(4qt - s + s_0)\right). \tag{3.9}$$

Consequently, from (2.20), we have that the total length of the Heisenberg curve is $\mathcal{L}(t) = 2\pi$.

Conversely, we can prove that a one-soliton solution of HF corresponding to the eigenvalue ia can be obtained from a one-soliton solution of NLS corresponding to the same eigenvalue ia. In other words, we want to show that the construction illustrated above, for obtaining a solution of NLS from a solution of HF equation, can be inverted, preserving the spectrum. We will do this in two alternative (equivalent) ways:

(1) Given the eigenvalue $ia = i(p + i\,q)$, we will construct the corresponding one-soliton solution of NLS (3.9); using the Hasimoto map (3.3), we will find the curvature $\tilde\kappa$ and the torsion $\tilde\tau$ of the corresponding Da Rios curve; we will write the Frenet-Serret system of equations (1.4) for the tangent, normal and binormal to the curve, where the tangent corresponds to the magnetization vector that solves HF; finally, using (3.5), we will construct the one-soliton solution of HF for the same eigenvalue $ia = i(p + i\,q)$ and we will prove that, if we interpret the magnetization

vector as the tangent vector to the Da Rios curve for NLS, then it solves the Frenet-Serret system for $\tilde{\kappa}$ and $\tilde{\tau}$.

(2) Given the eigenvalue $ia = i(p + i\,q)$, we will construct the corresponding one-soliton solution of NLS (3.9); using the Hasimoto map (3.3), we will find the curvature $\tilde{\kappa}$ and the torsion $\tilde{\tau}$ of the corresponding Da Rios curve; using the relation between a curve and the spherical indicatrix of its tangent, we will compute the curvature κ and the torsion τ of the corresponding spherical indicatrix, via (2.6); using (3.5), we will construct the one-soliton solution of HF for the same eigenvalue ia, representing a curve on the unit sphere; finally, we will compute the curvature κ and the torsion τ for the magnetization curve on the sphere and show that such κ and τ are the same curvature and torsion that we obtained for the spherical indicatrix.

Method 1: via Frenet-Serret. We start by constructing the one-soliton solution of NLS for the discrete eigenvalue ia, see equation (3.9):

$$u(s,t) = 2\,p e^{i(4p^2t+2q(-2qt+s)+\tilde{\phi}_0)}\,\operatorname{sech}\left(2p(4qt-s+s_0)\right).$$

The curvature $\tilde{\kappa}$ and the torsion $\tilde{\tau}$ of the corresponding Da Rios curve can be simply obtained from the formulae (3.6). We set the Frenet-Serret equations in the form: $U_s = FU$ where

$$F = \begin{pmatrix} 0 & \tilde{\kappa} & 0 \\ -\tilde{\kappa} & 0 & \tilde{\tau} \\ 0 & -\tilde{\tau} & 0 \end{pmatrix}, \quad U = \begin{pmatrix} \mathbf{t} \\ \mathbf{n} \\ \mathbf{b} \end{pmatrix} = \begin{pmatrix} t_1 & t_2 & t_3 \\ n_1 & n_2 & n_3 \\ b_1 & b_2 & b_3 \end{pmatrix}. \tag{3.10}$$

As U has to be an orthogonal matrix, it must satisfy the relation $U_s\,U^\dagger = F$. A solution U of the Frenet-Serret system is defined modulo a fixed rotation. Indeed, one immediately sees that, if U satisfies the Frenet-Serret system and R is a generic rotation, then the matrix $\hat{U} = U\,R$ also satisfies the same system of equations.

The one-soliton solution for HF corresponding to the same discrete eigenvalue $ia = i(p + i\,q)$ is given by equation (3.5). If we interpret the magnetization vector $\mathbf{m}$ as the tangent $\mathbf{t}$ to the Da Rios curve, we can easily check that

$$U = \begin{pmatrix} m_1 & m_2 & m_3 \\ n_1 & n_2 & n_3 \\ b_1 & b_2 & b_3 \end{pmatrix}, \tag{3.11a}$$

where

$$\mathbf{n} = \frac{\mathbf{t}_s}{\|\mathbf{t}_s\|} = \frac{1}{\kappa}\mathbf{t}_s\,, \quad \mathbf{b} = \mathbf{t} \times \mathbf{n}\,, \tag{3.11b}$$

satisfies the Frenet-Serret system in the form $U_s U^\dagger = F$.

Method 2: via the spherical indicatrix. We start again by constructing the one-soliton solution of NLS for the discrete eigenvalue ia, see equation (3.9):

$$u(s,t) = 2\,p e^{i(4p^2t+2q(-2qt+s)+\tilde{\phi}_0)}\,\operatorname{sech}\left(2p(4qt-s+s_0)\right).$$

The curvature $\tilde{\kappa}$ and the torsion $\tilde{\tau}$ of the corresponding Da Rios curve can be simply obtained from formulae (3.6) yielding

$$\tilde{\kappa} = 4p\operatorname{sech}\left(2p(4qt-s+s_0)\right), \quad \tilde{\tau} = 2q\,.$$

The curvature $\hat{\kappa}$ and the $\hat{\tau}$ of the corresponding spherical indicatrix of the tangent to the above Da Rios curve can be immediately obtained from formulae (2.6), giving

$$\hat{\kappa} = \frac{1}{2p}\cosh\left(2p(4qt - s + s_0)\right)\sqrt{q^2 + 4p^2\operatorname{sech}^2\left(2p(4qt - s + s_0)\right)}\,, \tag{3.12}$$

$$\hat{\tau} = -\frac{pq\tanh\left(2p(4qt - s + s_0)\right)}{q^2 + 4p^2\operatorname{sech}^2\left(2p(4qt - s + s_0)\right)}\,. \tag{3.13}$$

The one-soliton solution for HF corresponding to the same discrete eigenvalue ia is given by equation (3.5). The curvature κ and the torsion τ of the magnetization $\mathbf{m}$ are given by (3.1b). It is just the matter of a direct computation to see that the curvature κ and the torsion τ of the magnetization curve coincide with $\hat{\kappa}$ and $\hat{\tau}$ if $q > 0$ or with $\hat{\kappa}$ and $-\hat{\tau}$ if $q < 0$. As the velocity of the NLS soliton is $4q$, the change of sign of q entails a change of direction on the Da Rios curve, and thus a change of sign of the torsion.

3.2. **Connecting Da Rios to Heisenberg curves in the reflectionless case.** All reflectionless solutions of NLS (2.1) and HF (1.2) can be conveniently given in explicit form and classified by means of the so-called matrix-triplet method, as illustrated in [6] and [24]. Before exploiting the geometric connection realized by the spherical indicatrix map $\mathcal{B}$ with the aim of constructing a localized (soliton) solution of the HF equation starting from a reflectionless solution of the NLS equation and viceversa, we briefly summarize here the matrix-triplet formulae for NLS and HF as obtained in [6] and [24], respectively.

In order to construct a reflectionless solution of both equations, one requires a matrix triplet (A, B, C) satisfying the following hypotheses:

(1) A is an $\bar{n} \times \bar{n}$ complex matrix featuring $n \leq \bar{n}$ distinct eigenvalues $\{a_j\}_{j=1}^n$: the geometric multiplicity of the eigenvalues is 1; the algebraic multiplicity of each eigenvalue a_j is $n_j \geq 1$, so that $\bar{n} = \sum_{j=1}^n n_j$; finally, all eigenvalues have positive real parts, $\operatorname{Re}(a_j) > 0$ for all j. The square matrix A is completely arbitrary, save for the *minimality* condition (see below) and for the above conditions on its eigenvalues.
(2) B is an $\bar{n} \times 1$ complex matrix, which can be chosen – without any loss of generality – to be an all-ones matrix.
(3) C is a $1 \times \bar{n}$ complex matrix. Again, C is completely arbitrary, save for the *minimality* condition (see below).
(4) The triplet (A, B, C) is a *minimal* triplet in the sense that the matrix order of A is minimal among all triplets representing the same Marchenko kernel as it appears in the IST set up for the integrable equation to which the matrix-triplet method is applied (see [84, 6, 24]).

The matrices A and C encode the discrete spectrum of the problem to which the method is applied (see [6] and [24]): in particular, for both NLS and HF, if $\{a_j\}_{j=1}^n$ are the eigenvalues of the square matrix A, then $\{ia_j\}_{j=1}^n$ are the poles of the transmission coefficient in the upper half-plane $\mathbb{C}^+$ (these are usually referred to as the *discrete eigenvalues* in the IST literature); moreover, the $\bar{n}$ elements of the rectangular matrix C correspond to the so-called *norming constants*.

It is not restrictive (in fact, it is the typical choice) to set the triplet (A, B, C) as follows [84]:

$$A_{\bar{n}\times\bar{n}} = \begin{pmatrix} A_1 & 0 & \cdots & 0 \\ 0 & A_2 & \cdots & 0 \\ \vdots & \vdots & \ddots & \vdots \\ 0 & 0 & \cdots & A_n \end{pmatrix}, \quad B_{\bar{n}\times 1} = \begin{pmatrix} B_1 \\ B_2 \\ \vdots \\ B_n \end{pmatrix}, \; C_{1\times\bar{n}} = \begin{pmatrix} C_1 & C_2 & \cdots & C_n \end{pmatrix}, \tag{3.14a}$$

where A is in Jordan canonical form, with A_j being the Jordan block of dimension $n_j \times n_j$ corresponding to the eigenvalue a_j,

$$A_j = \begin{cases} a_j & \text{if } n_j = 1 \\ \begin{pmatrix} a_j & 1 & 0 & 0 \\ 0 & \ddots & \ddots & 0 \\ 0 & 0 & \ddots & 1 \\ 0 & 0 & 0 & a_j \end{pmatrix} & \text{if } n_j > 1\,; \end{cases} \tag{3.14b}$$

B_j is a column vector of dimension n_j, typically chosen to be a vector of ones; and C_j is a row vector of dimension n_j,

$$C_j = \begin{pmatrix} c_{j,0} & c_{j,1} & \cdots & c_{j,n_j-1} \end{pmatrix}. \tag{3.14c}$$

Note that, due to the minimality, if the triplet (A, B, C) is set as in (3.14), then A features no repeated blocks on the main diagonal.

Given the matrix triplet (A, B, C), then two $\bar{n} \times \bar{n}$ auxiliary matrices, N and Q, are constructed as the solutions of the following matrix Lyapunov equations:

$$A^\dagger Q + QA = C^\dagger C\,, \quad AN + NA^\dagger = BB^\dagger\,, \tag{3.15a}$$

so that

$$N = \int_0^\infty \mathrm{d}z e^{-zA} BB^\dagger e^{-zA^\dagger}\,, \quad Q = \int_0^\infty \mathrm{d}z e^{-zA^\dagger} C^\dagger C e^{-zA}. \tag{3.15b}$$

By the minimality of the triplet (A, B, C), one can prove [84] that N and Q are positive Hermitian matrices, $N = N^\dagger$ and $Q = Q^\dagger$, where the dagger symbol $\dagger$ indicates the usual Hermitian adjoint.

Let $(A_{\mathrm{NLS}}, B_{\mathrm{NLS}}, C_{\mathrm{NLS}})$ be a choice of the matrix triplet as in (3.14), intended for the construction of a reflectionless solution of NLS. Let N_{NLS} and Q_{NLS} be the corresponding matrices N and Q, constructed as in (3.15) from $(A_{\mathrm{NLS}}, B_{\mathrm{NLS}}, C_{\mathrm{NLS}})$. Let $\tilde{B}_{\mathrm{NLS}}$, $\tilde{C}_{\mathrm{NLS}}$, $\tilde{N}_{\mathrm{NLS}}$, and $\tilde{Q}_{\mathrm{NLS}}$ be the following matrix-valued functions

$$\begin{aligned} \tilde{B}_{\mathrm{NLS}} \equiv \tilde{B}_{\mathrm{NLS}}(s) = e^{-sA_{\mathrm{NLS}}} B_{\mathrm{NLS}}\,, \quad \tilde{C}_{\mathrm{NLS}} \equiv \tilde{C}_{\mathrm{NLS}}(s,t) = C_{\mathrm{NLS}} e^{-sA_{\mathrm{NLS}}} e^{-4\,i\,t A_{\mathrm{NLS}}^2}\,, \\ \tilde{N}_{\mathrm{NLS}} \equiv \tilde{N}_{\mathrm{NLS}}(s) = e^{-sA_{\mathrm{NLS}}} N_{\mathrm{NLS}} e^{-sA_{\mathrm{NLS}}^\dagger} = \tilde{N}_{\mathrm{NLS}}^\dagger\,, \\ \tilde{Q}_{\mathrm{NLS}} \equiv \tilde{Q}_{\mathrm{NLS}}(s,t) = e^{4\,i\,t A_{\mathrm{NLS}}^{\dagger 2}} e^{-s\,A_{\mathrm{NLS}}^\dagger} Q_{\mathrm{NLS}} e^{-sA_{\mathrm{NLS}}} e^{-4itA_{\mathrm{NLS}}^2} = \tilde{Q}_{\mathrm{NLS}}^\dagger\,. \end{aligned} \tag{3.16}$$

Finally, let $\tilde{\Gamma}_{\mathrm{NLS}}$ be the following matrix-valued function

$$\tilde{\Gamma}_{\mathrm{NLS}} \equiv \tilde{\Gamma}_{\mathrm{NLS}}(s,t) = I_{\bar{n}} + \tilde{Q}_{\mathrm{NLS}} \tilde{N}_{\mathrm{NLS}}\,, \quad \text{so that} \quad \tilde{\Gamma}_{\mathrm{NLS}}^\dagger = I_{\bar{n}} + \tilde{N}_{\mathrm{NLS}} \tilde{Q}_{\mathrm{NLS}}\,, \tag{3.17}$$

where $I_{\bar{n}}$ is the $\bar{n} \times \bar{n}$ identity matrix.

Then, a reflectionless (soliton) solution $u(s,t)$ of (2.1) reads [6]:

$$u(s,t) = -2\tilde{B}_{\mathrm{NLS}}^\dagger \tilde{\Gamma}_{\mathrm{NLS}}^{-1} \tilde{C}_{\mathrm{NLS}}^\dagger = \frac{\det\left(\tilde{\Gamma}_{\mathrm{NLS}} - 2\tilde{C}_{\mathrm{NLS}}^\dagger \tilde{B}_{\mathrm{NLS}}^\dagger\right)}{\det(\tilde{\Gamma}_{\mathrm{NLS}})} - 1\,. \tag{3.18}$$

On the other hand, to construct a solution of the HF equation (1.2), we start by casting a choice $(A_{\rm HF}, B_{\rm HF}, C_{\rm HF})$ of the matrix triplet as in (3.14). Then we build the matrix-valued functions $\tilde{B}_{\rm HF}$, $\tilde{C}_{\rm HF}$, $\tilde{N}_{\rm HF}$, and $\tilde{Q}_{\rm HF}$ analogously to what we have done for the case of NLS, using the same expressions (3.2). Finally, we define the matrix-valued function $\tilde{\Gamma}_{\rm HF} \equiv \tilde{\Gamma}_{\rm HF}(s,t) = I_{\bar{n}} + \tilde{Q}_{\rm HF}\tilde{N}_{\rm HF}$ exactly as in the NLS case.

Then, a reflectionless (soliton) solution $\mathbf{m}(s,t) = \sum_{j=1}^{3} m_j(s,t)\,\mathbf{e}_j$ of (1.2) reads [24]:

$$m_1(s,t) + i\,m_2(s,t) = -2\,(1+L_1)\,L_2\,, \quad m_3(s,t) = 2\,|1+L_1|^2 - 1\,, \tag{3.19a}$$

where the scalar functions $L_1 \equiv L_1(s,t)$ and $L_2 \equiv L_2(s,t)$ are given by

$$\begin{aligned} L_1 &= -\tilde{C}_{\rm HF}\tilde{N}_{\rm HF}\tilde{\Gamma}_{\rm HF}^{-1}A^{\dagger^{-1}}\tilde{C}_{\rm HF}^{\dagger} = \frac{\det\left(I_{\bar{n}} - A^{\dagger^{-1}}\tilde{Q}_{\rm HF}A\tilde{N}_{\rm HF}\right)}{\det(\tilde{\Gamma}_{\rm HF})} - 1\,, \\ L_2 &= \tilde{B}_{\rm HF}\tilde{\Gamma}_{\rm HF}^{-1}A^{\dagger^{-1}}\tilde{C}_{\rm HF}^{\dagger} = \frac{\det\left(\tilde{\Gamma}_{\rm HF} + A^{\dagger^{-1}}\tilde{C}_{\rm HF}^{\dagger}\tilde{B}_{\rm HF}^{\dagger}\right)}{\det(\tilde{\Gamma}_{\rm HF})} - 1\,. \end{aligned} \tag{3.19b}$$

In Appendix 5, alternative formulae for $u(s,t)$ and for $\mathbf{m}(s,t)$, along with their time and space derivatives, are provided in forms that are easier to handle than (3.18) and (3.19) in view of their numerical evaluations.

Now we are ready to show the preservation of the localization for the spherical indicatrix map $\mathcal{B}$ in the general reflectionless case. Indeed, from equation (3.3), we know that the spherical indicatrix map entails $2\,|u| = \|\mathbf{m}_s\|$. Using the explicit expressions of the reflectionless solutions of NLS and HF, (3.18) and (3.19), respectively, then, after a tedious and rather cumbersome computation, we obtain

$$|u|^2 = \mathrm{tr}\big[\tilde{\Gamma}_{\rm NLS}^{-1}\frac{\partial}{\partial s}\tilde{\Gamma}_{\rm NLS}\big]_s \quad \text{and} \quad \|\mathbf{m}_s\|^2 = \frac{1}{4}\mathrm{tr}\big[\tilde{\Gamma}_{\rm HF}^{-1}\frac{\partial}{\partial s}\tilde{\Gamma}_{\rm HF}\big]_s\,. \tag{3.20}$$

Formulae (3.20) show that, if we take a matrix triplet (A,B,C) and we use it to construct a solution of HF according to (3.19), so that $A_{\rm HF} = A$, $B_{\rm HF} = B$, $C_{\rm HF} = C$, then the solution of NLS that we get via the spherical indicatrix map $\mathcal{B}$ features the very same norm that we would have obtained had we used directly the same matrix triplet (A,B,C) in the NLS solution formula (3.18), namely with $A_{\rm NLS} = A$, $B_{\rm NLS} = B$, $C_{\rm NLS} = C$. Conversely, if we take a matrix triplet (A,B,C) and we use it to construct a solution of NLS according to (3.18), so that $A_{\rm NLS} = A$, $B_{\rm NLS} = B$, $C_{\rm NLS} = C$, then the solution of HF that we get via the spherical indicatrix map $\mathcal{B}$ features the very same norm of the spatial derivative that we would have obtained had we used directly the same matrix triplet (A,B,C) in the HF solution formula (3.19), namely with $A_{\rm HF} = A$, $B_{\rm HF} = B$, $C_{\rm HF} = C$.

In the following, we provide four examples of localized solutions of HF built from reflectionless solutions of NLS and viceversa, utilizing the spherical indicatrix map $\mathcal{B}$ as described in Section 3.1. In particular, in order to construct a localized solution of HF from a reflectionless solution of NLS we proceed as follows.

(1) We choose a matrix triplet $(A_{\rm NLS}, B_{\rm NLS}, C_{\rm NLS})$ and we construct, via (3.18), the corresponding solution of NLS, $u(s,t)$.
(2) We specialize the solution at $t = 0$, $u(s,0)$, and we compute the curvature $\tilde{\kappa}(s,0)$ and the torsion $\tilde{\tau}(s,0)$ of the corresponding Da Rios curve via the Hasimoto map (3.3).

(3) We evaluate the Frenet-Serret frame, ($\mathbf{t}$, $\mathbf{n}$, $\mathbf{b}$), along the Da Rios curve characterized by the curvature $\tilde{\kappa}(s,0)$ and the torsion $\tilde{\tau}(s,0)$, by integrating numerically, for all s in a given interval $[s_1, s_2]$ and at $t = 0$, the Frenet-Serret system (1.4) with initial condition

$$\begin{pmatrix} \mathbf{t} \\ \mathbf{n} \\ \mathbf{b} \end{pmatrix}_{s=s_1} = \begin{pmatrix} 0 & 0 & 1 \\ 1 & 0 & 0 \\ 0 & 1 & 0 \end{pmatrix} . \tag{3.21}$$

From identity (2.5), we know that the vector $\mathbf{t}$ obtained in this manner corresponds to the magnetization at $t = 0$, $\mathbf{t} = \mathbf{m}(s,0)$. If the numerical integration is carried out in the finite interval $[s_1, s_2]$, then the choice of the initial condition (3.21) entails a rigid translation of the magnetization at infinity to $s = s_1$. For this reason, the numerical values of s_1 and s_2 are chosen in such a way that, for those values, the Da Rios curve be approximately a straight line (namely, $\tilde{\kappa}(s_1,0) \approx \tilde{\kappa}(s_2,0) \approx 0$), so that the magnetization $\mathbf{m}$, which is exactly $\mathbf{e}_3$ at $s = s_1$ because of (3.21), be also close to $\mathbf{e}_3$ at $s = s_2$. We remind here that the HF equation (1.2) is invariant under translations. The numerical integration is carried out by means of the adaptive, seven-stage Dormand-Prince $(4,5)$ embedded Runge-Kutta method, implemented as part of a Matlab R2017a routine.

(4) Finally, we integrate numerically the HF equation (1.2) with initial condition $\mathbf{m}(s,0)$, as obtained above, using the method of lines with a pseudospectral, Fourier discretization in space and the same adaptive Dormand-Prince method for the time stepping, all implemented in a single Matlab R2017a routine. It is worth observing here that the above procedure for producing $\mathbf{m}(s,0)$ cannot be repeated for all points in time, as the choice of the initial condition would imply a different translation of the magnetization at infinity.

On the other hand, to construct a localized solution of NLS from a reflectionless solution of HF we proceed as follows.

(1) We choose a matrix triplet $(A_{\mathrm{HF}}, B_{\mathrm{HF}}, C_{\mathrm{HF}})$ and we construct, via (3.19), the corresponding solution of HF.
(2) Via (3.3), we find the curvature $\tilde{\kappa}(s,t)$ and $\tilde{\tau}(s,t)$ of the Da Rios curve whose spherical indicatrix on $\mathcal{S}^2$ is the Heisenberg curve $\mathbf{m}(s,t)$.
(3) Finally, we use the Hasimoto map (3.4a) to reconstruct a solution of the NLS equation (2.1).

Figure 3 illustrates a one-soliton solution of NLS utilized to construct a one-soliton solution of HF and viceversa. The one-soliton solution of NLS in Figure 3(a) is obtained, via (3.18), from the following matrix triplet:

$$A = (a)\,, \quad B = (1)\,, \quad C = (c)\,, \tag{3.22a}$$

with

$$a = \frac{\sqrt{7}+i}{4}\,, \quad c = \frac{-7+i3\sqrt{7}}{8} e^{-2(\sqrt{7}+i)}\,. \tag{3.22b}$$

Similarly, the one-soliton solution of HF in Figure 3(d) is obtained, via (3.19), from the same matrix triplet (3.22). Here $\bar{n} = n = 1$ and the matrix A is a scalar. As shown in [6], if this matrix triplet is employed to construct a one-soliton solution of NLS, then the soliton obtained propagates with velocity $V = 4\,\mathrm{Im}(a) = 1$ and

has amplitude $2\,\mathrm{Re}(a) = \frac{\sqrt{7}}{2}$. On the other hand, as shown in [24], if this matrix triplet is used to construct a one-soliton solution of HF, then the soliton obtained propagates with the same velocity $V = 4\,\mathrm{Im}(a) = 1$ of the NLS soliton and is characterized by the precession frequency $\omega = 4|a|^2 = 2$. Figures 3(b) and 3(c) show the corresponding solutions of HF and NLS, respectively, as obtained from the given solution of NLS and HF, respectively, via the spherical indicatrix map $\mathcal{B}$. The relevant Da Rios and Heisenberg curves are illustrated, at different times, in Figure 7(a), along with the evolution of the length of the Heisenberg curve, which, in this case, keeps the constant value of 2π, as expected.

Figure 4 illustrates a two-soliton solution of NLS utilized to construct a two-soliton solution of HF and viceversa. The two-soliton solution of NLS in Figure 4(a) is obtained, via (3.18), from the matrix triplet:

$$\begin{gathered} A = \begin{pmatrix} \frac{\sqrt{7}+i}{4} & 0 \\ 0 & \frac{\sqrt{7}-i}{4} \end{pmatrix}, \quad B = \begin{pmatrix} 1 \\ 1 \end{pmatrix}, \\ C = \begin{pmatrix} \frac{-7+i3\sqrt{7}}{8} e^{-5(\sqrt{7}+i)/2} & \frac{-3\sqrt{7}+i7}{8} e^{-5(\sqrt{7}-i)/2} \end{pmatrix}. \end{gathered} \tag{3.23}$$

Similarly, the two-soliton solution of HF in Figure 4(d) is obtained, via (3.19), from the same matrix triplet (3.23). Here $\bar{n} = n = 2$, and the matrix A features two distinct eigenvalues. The relevant Da Rios and Heisenberg curves are illustrated, at different times, in Figure 7(b), along with the evolution of the length of the Heisenberg curve. We observe two loop solitons propagating and interacting along the Da Rios curve. When the HF solitons are well separated in space, the magnetization in the region between them is close to the asymptotic magnetization $\mathbf{e}_3$, and the Heisenberg curve is formed by two (almost overlapped and almost indistinguishable, for this choice of the matrix triplet) branches, each one of them starting and ending at the north pole of $\mathcal{S}^2$. As long as the two HF solitons get close to each other enough, the magnetization in the region between them moves more and more away from the asymptotic state $\mathbf{e}_3$, and the Heisenberg curve does not pass twice through the north pole, turning into a single branch: its length decreases as the solitons get close to one another, reaches a minimum at the centre of the interaction, and then increases again as the solitons separate.

Figure 5 illustrates a two-pole solution of NLS utilized to construct a two-pole solution of HF and viceversa. The two-pole solution of NLS in Figure 5(a) is obtained, via (3.18), from the matrix triplet

$$A = \begin{pmatrix} \sqrt{2} & 1 \\ 0 & \sqrt{2} \end{pmatrix}, \quad B = \begin{pmatrix} 1 \\ 1 \end{pmatrix}, \quad C = \begin{pmatrix} 8 & 4\sqrt{2}(1-\sqrt{2}) \end{pmatrix}. \tag{3.24}$$

Similarly, the two-pole solution of HF in Figure 5(d) is obtained, via (3.19), from the same matrix triplet (3.24). Here $\bar{n} = 2$ and $n = 1$, and the matrix A is in Jordan form, thus it features one eigenvalue with algebraic multiplicity 2 (that is why the corresponding solution is called a "two-pole" solution). The relevant Da Rios and Heisenberg curves are illustrated, at different times, in Figure 8(a), along with the evolution of the length of the Heisenberg curve. The general behaviour is similar to that of the two solitons case, however, at the maximum of the interaction, the two loop solitons along the Da Rios curve form a super-loop, namely a loop-over-a-loop. The length of the Heisenberg curve shows a cusp at the time of maximum interaction.

Figure 6 illustrates a breather-like solution of NLS utilized to construct a breather-like solution of HF and viceversa. The breather-like solution of NLS in Figure 6(a) is obtained, via (3.18), from the matrix triplet

$$A = \begin{pmatrix} \frac{1}{\sqrt{5}} & 0 \\ 0 & \frac{1}{\sqrt{10}} \end{pmatrix}, \quad B = \begin{pmatrix} 1 \\ 1 \end{pmatrix}, \quad C = \begin{pmatrix} 2\sqrt{\frac{17+12\sqrt{2}}{5}} & \sqrt{2}\sqrt{\frac{17+12\sqrt{2}}{5}} \end{pmatrix}. \quad (3.25)$$

Similarly, the breather-like solution of HF in Figure 6(d) is obtained, via (3.19), from the same matrix triplet (3.25). Like in the two soliton case, here $\bar{n} = n = 2$, and the matrix A features two distinct eigenvalues. The conditions for the existence of an oscillating, breather-like solution (which is formed by two entangled propagating or stationary solutions) are dictated by the norming constant matrix C, see [24]. In particular, with this choice of the values in the matrix triplet, we expect a periodic solution with period $5\,\pi \approx 15.7080$ (see [24]). The relevant Da Rios and Heisenberg curves are illustrated, at different times, in Figure 8(b), along with the evolution of the length of the Heisenberg curve. The breather on the Da Rios curve is an oscillating structure formed by two loop solitons, periodically attracting, interacting and overtaking each other. Like in the case of the two-pole solution, we observe the (periodic) formation of a super-loop along the Da Rios curve at the maximum of the interaction of the two solitons forming the breather.

In all the examples, as expected from (3.20), the solution of HF that we obtain from a reflectionless solution of NLS corresponding to a matrix triplet (A, B, C) via (3.18) is the same that we would have obtained had we used directly the same matrix triplet (A, B, C) in the HF solution formula (3.19), see Figures 3(a) and 3(b), Figures 4(a) and 4(b), Figures 5(a) and 5(b), and Figures 6(a) and 6(b). Similarly, in all the examples, the solution of NLS that we obtain from a reflectionless solution of HF corresponding to a matrix triplet (A, B, C) via (3.19) is the same (modulo a phase shift) that we would have obtained had we used directly the same matrix triplet (A, B, C) in the NLS solution formula (3.18), see Figures 3(d) and 3(c), Figures 4(d) and 4(c), Figures 5(d) and 5(c), and Figures 6(d) and 6(c). This confirms that the spherical indicatrix map $\mathcal{B}$ preserves the localization and the typology of the solutions on which it acts, namely it maps reflectionless solutions of HF to the same typology of reflectionless solutions of NLS and viceversa.

4. Conclusions and outlooks

In this paper we have studied the properties of the spherical curve associated to the Heisenberg equations. The natural variables for the description of this curve motion are the geodesic curvature K and the arc-length σ which are related to the magnetic vector $\mathbf{m}$ by (2.24),

$$K = \|\mathbf{m} + \mathbf{m}_{\sigma\sigma}\|, \quad \sigma_s = \|\mathbf{m}_s\|,$$

where s is a time independent curve parameterization. Our study is based on the geometrical relation between the binormal-velocity motion of a curve (Da Rios model) and the induced motion on the related spherical indicatrix (HF model). While the binormal motion is purely geometrical, being the evolution of curvature and torsion, which is independent from the chosen curve parameterization, the induced spherical motion depends on the "metric" on the curve. This is the reason of the main geometrical difference between the two curve motions: the Da Rios case is associated to a non-stretching curve (featuring time-independent arc-lenght), whereas

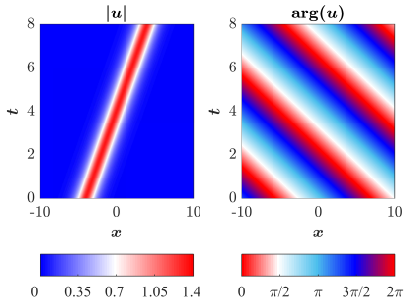

(a) One-soliton solution of the NLS equation (2.1) obtained directly via (3.18) with the matrix triplet (3.22).

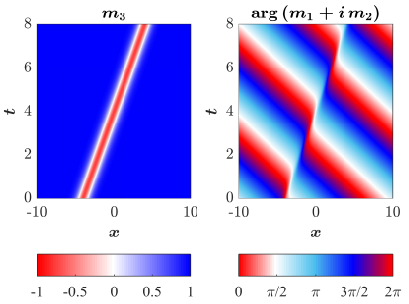

(b) Solution of the HF equation (1.2) generated via the map $\mathcal{B}$ from the one-soliton solution of the NLS equation, the latter having been obtained via (3.18) with the matrix triplet (3.22).

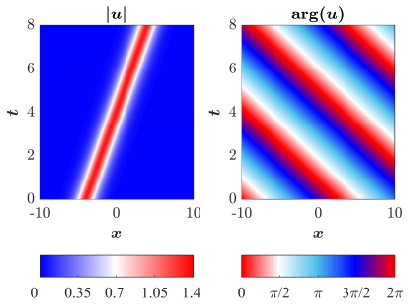

(c) Solution of the NLS equation generated via the (inverse) map $\mathcal{B}$ from the one-soliton solution of the HF equation, the latter having been obtained via (3.19) with the matrix triplet (3.22).

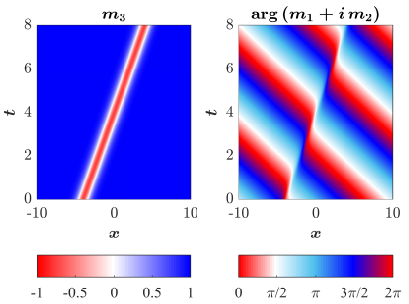

(d) One-soliton solution of the HF equation obtained directly via (3.19) with the matrix triplet (3.22).

Figure 3: Preservation of the spectrum and of the localization from the application of the spherical indicatrix map $\mathcal{B}$ between a one-soliton solution of the NLS equation (2.1) and a one-soliton s olution of the HF equation (1.2). The corresponding Da Rios and Heisenberg curves are illustrated in Figure 7(a).

the HF case is related to a stretching curve. As a consequence the total length of the spherical curve associated to the Heisenberg motion is not constant: this gives a possible indication on the behavior of the mean value of the spin variation. Moreover, this geometrical interpretation of the classical mapping between Da Rios and HF simplifies computationally the study of qualitative features of the localized solutions on the spherical curve (breathers, solitons, multipoles, and mixed combinations among them).

Finally, as already remarked in the paper, we recall that many hydrodynamic models of ferromagnetism has been proposed (see, for instance, [78, 83, 69, 42]),

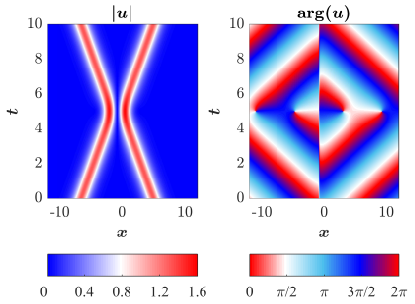

(a) Two-soliton solution of the NLS equation obtained directly via (3.18) with the matrix triplet (3.23).

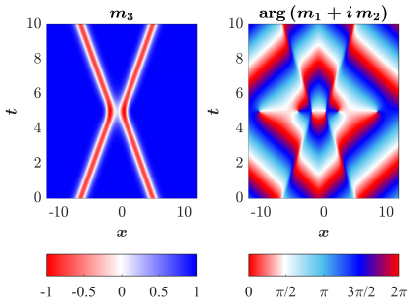

(b) Solution of the HF equation generated via the map $\mathcal{B}$ from the two-soliton solution of the NLS equation, the latter having been obtained via (3.18) with the matrix triplet (3.23).

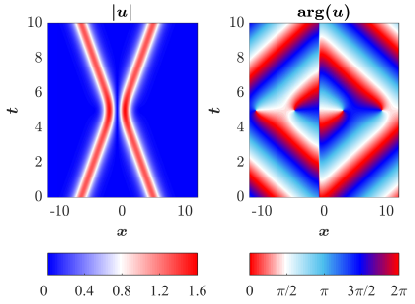

(c) Solution of the NLS equation generated via the (inverse) map $\mathcal{B}$ from the two-soliton solution of the HF equation, the latter having been obtained via (3.19) with the matrix triplet (3.23).

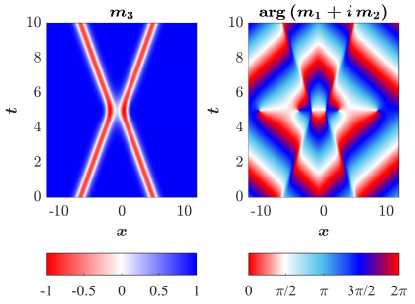

(d) Two-soliton solution of the HF equation obtained directly via (3.19) with the matrix triplet (3.23).

Figure 4: Preservation of the spectrum and of the localization from the application of the spherical indicatrix map $\mathcal{B}$ between a two-soliton solution of the NLS equation (2.1) and a two-soliton solution of the HF equation (1.2). The corresponding Da Rios and Heisenberg curves are illustrated in Figure 7(b).

mainly in two or three dimensions: the hydrodynamic reduction of HF presented here, even if simplified as it is one-dimensional in space, has the peculiar feature of connecting Heisenberg ferromagnetism directly to geometrical objects, using intrinsic variables.

This work opens a promising outlook on the study of the theoretical (and potentially also experimental) repercussions of the notion of gradient catastrophe in the context of ferromagnetism.

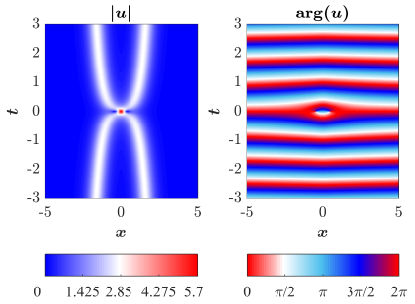

(a) Two-pole solution of the NLS equation obtained directly via (3.18) with the matrix triplet (3.24).

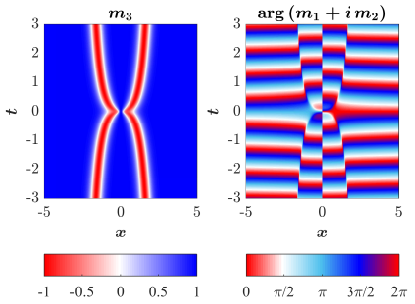

(b) Solution of the HF equation generated via the map $\mathcal{B}$ from the two-pole solution of the NLS equation, the latter having been obtained via (3.18) with the matrix triplet (3.24).

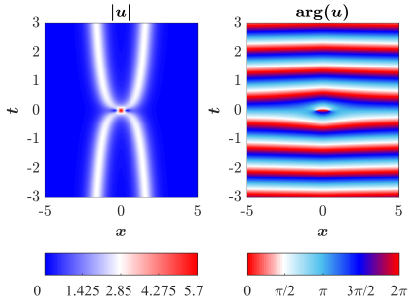

(c) Solution of the NLS equation generated via the (inverse) map $\mathcal{B}$ from the two-pole solution of the HF equation, the latter having been obtained via (3.19) with the matrix triplet (3.24).

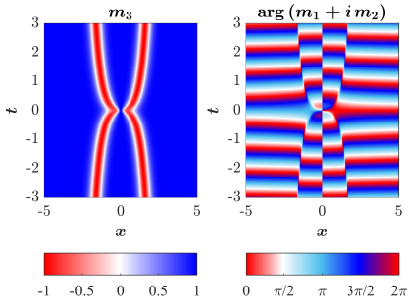

(d) Two-pole solution of the HF equation obtained directly via (3.19) with the matrix triplet (3.24).

Figure 5: Preservation of the spectrum and of the localization from the application of the spherical indicatrix map $\mathcal{B}$ between a two-pole solution of the NLS equation (2.1) and a two-pole solution of the HF equation (1.2). The corresponding Da Rios and Heisenberg curves are illustrated in Figure 8(a).

5. Appendix

In this appendix we provide formulae alternative to (3.18) and (3.19) for the numerical evaluation of the solutions of NLS and HF, respectively, along with their space and time derivatives. For the sake of simplicity, in this section we drop the subscripts NLS or HF from the matrix triplets (A, B, C) and from the auxiliary matrices N, Q, and Γ. In particular, given the matrix triplet (A, B, C) according to (3.14), we consider the matrix-valued function

$$C(t) = Ce^{-4itA^2} = \tilde{C}(0, t)\,, \tag{5.1a}$$

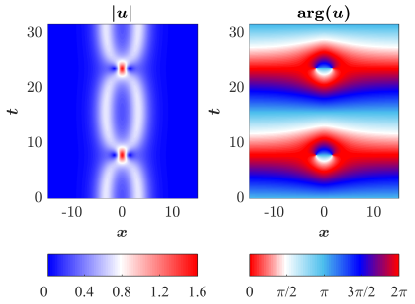

(a) Breather-like solution of the NLS equation obtained directly via (3.18) with the matrix triplet (3.25).

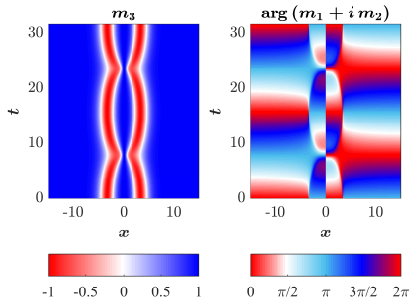

(b) Solution of the HF equation generated via the map $\mathcal{B}$ from the breather-like solution of the NLS equation, the latter having been obtained via (3.18) with the matrix triplet (3.25).

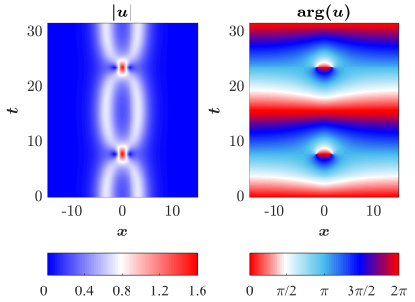

(c) Solution of the NLS equation generated via the (inverse) map $\mathcal{B}$ from the breather-like solution of the HF equation, the latter having been obtained via (3.19) with the matrix triplet (3.25).

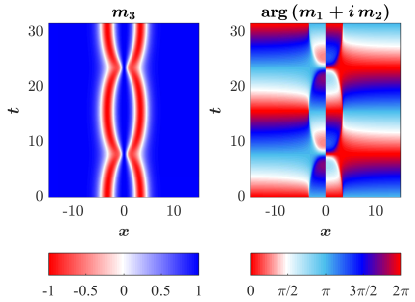

(d) Breather-like solution of the HF equation obtained directly via (3.19) with the matrix triplet (3.25).

Figure 6: Preservation of the spectrum and of the localization from the application of the spherical indicatrix map $\mathcal{B}$ between a breather-like solution of the NLS equation (2.1) and a breather-like solution of the HF equation (1.2). The corresponding Da Rios and Heisenberg curves are illustrated in Figure 8(b).

along with the auxiliary matrix N, and the matrix-valued function $Q(t)$,

$$Q(t) = (e^{-4itA^2})^\dagger Q e^{-4itA^2} = \tilde{Q}(0,t)\,. \tag{5.1b}$$

5.1. **Alternative formulations of the solution of NLS and its space and time derivatives.** Formula (3.18) can be rewritten as

$$u(s,t) = -2\tilde{B}^\dagger \tilde{\Gamma}^{-1}\tilde{C}^\dagger = \frac{\det\left(\tilde{\Gamma} - 2\tilde{C}^\dagger \tilde{B}^\dagger\right)}{\det(\tilde{\Gamma})} - 1$$

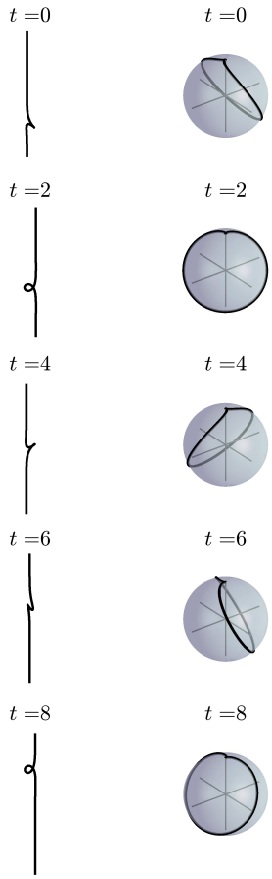

(a) Time evolution of the Heisenberg curve (right) for the one-soliton solution of HF obtained via (3.19) with the matrix triplet (3.22), see Figure 3(d), alongside that of the Da Rios curve (left) for the corresponding one-soliton solution of NLS, as obtained via the spherical indicatrix map $\mathcal{B}$, see Figure 3(c).

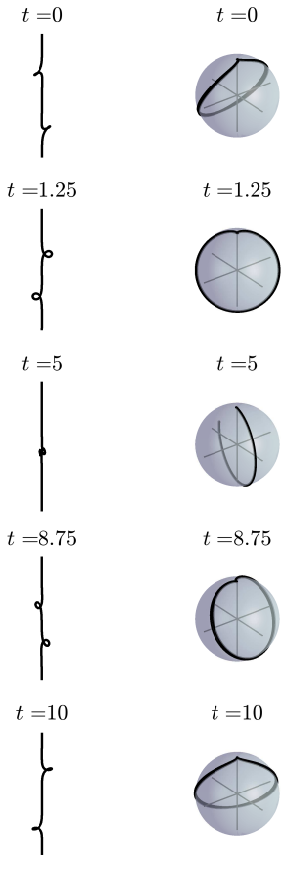

(b) Time evolution of the Heisenberg curve (right) for the two-soliton solution of HF obtained via (3.19) with the matrix triplet (3.23), see Figure 4(d), alongside that of the Da Rios curve (left) for the corresponding two-soliton solution of NLS, as obtained via the spherical indicatrix map $\mathcal{B}$, see Figure 4(c).

Figure 7: Time evolutions of corresponding Da Rios and Heisenberg curves for the one-soliton and two-soliton solutions.

$$= \frac{\det\left(e^{2sA^\dagger}N^{-1}e^{2sA} + Q(t) - 2C(t)^\dagger B^\dagger N^{-1}e^{2sA}\right)}{\det\left(e^{2sA^\dagger}N^{-1}e^{2sA} + Q(t)\right)} - 1 \tag{5.2a}$$

$$= \frac{\det\left(N^{-1} + e^{-2sA^\dagger}Q(t)e^{-2sA} - 2e^{-2sA^\dagger}C(t)^\dagger B^\dagger N^{-1}\right)}{\det\left(N^{-1} + e^{-2sA^\dagger}Q(t)e^{-2sA}\right)} - 1\,, \tag{5.2b}$$

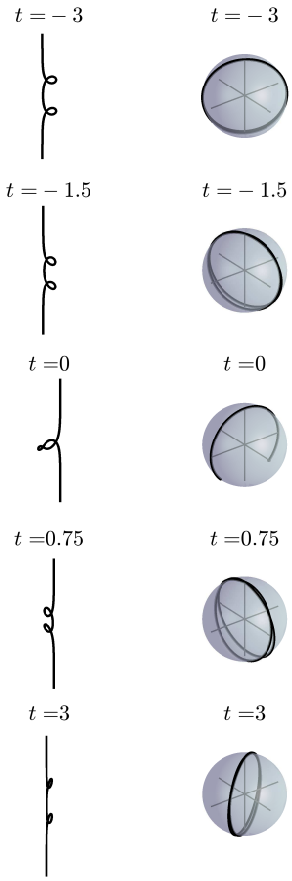

(a) Time evolution of the Heisenberg curve (right) for the two-pole solution of HF obtained via (3.19) with the matrix triplet (3.24), see Figure 5(d), alongside that of the Da Rios curve (left) for the corresponding two-pole solution of NLS, as obtained via the spherical indicatrix map $\mathcal{B}$, see Figure 5(c).

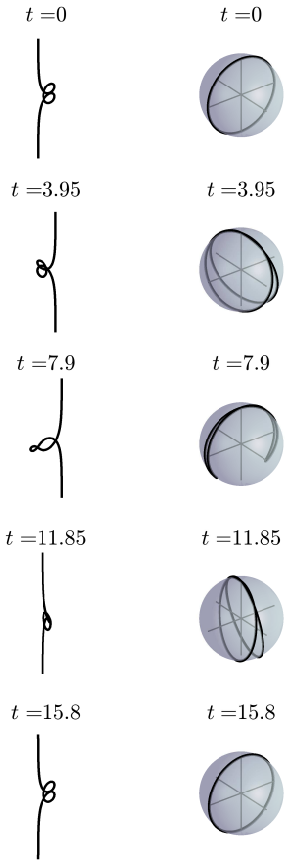

(b) Time evolution of the Heisenberg curve (right) for the breather-like solution of HF obtained via (3.19) with the matrix triplet (3.25), see Figure 6(d), alongside that of the Da Rios curve (left) for the corresponding breather-like solution of NLS, as obtained via the spherical indicatrix map $\mathcal{B}$, see Figure 6(c).

Figure 8: Time evolutions of corresponding Da Rios and Heisenberg curves for the two-pole and breather-like solutions.

where expression (5.2a) is convenient for evaluating numerically $u(s,t)$ when $s \leq 0$, whereas (5.2b) is convenient for evaluating numerically $u(s,t)$ when $s \geq 0$.

Similarly, for the space derivative, we get

$$\frac{\partial}{\partial s}u(s,t) = 4\tilde{B}^{\dagger}\tilde{\Gamma}^{-1}\big[A^{\dagger} - \tilde{Q}A\tilde{N}\big]\tilde{\Gamma}^{-1}\tilde{C}^{\dagger}$$

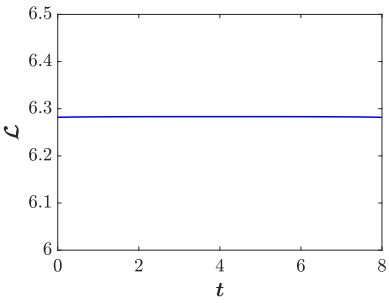

(a) One-soliton solution, see Fig. 7(a)

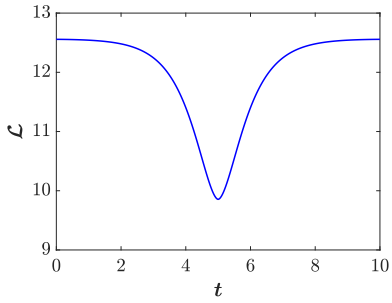

(b) Two-soliton solution, see Fig. 7(b)

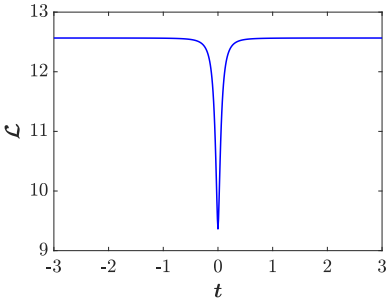

(c) Two-pole solution, see Fig. 8(a)

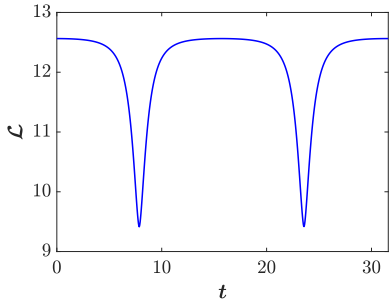

(d) Breather solution, see Fig. 8(b)

Figure 9: $\mathcal{L}(t)$, length of the Heisenberg curve, for the cases illustrated in Figures 7 and 8.

$$
\begin{aligned}
&= \frac{\det\left(\tilde{\Gamma}[A^\dagger - \tilde{Q}A\tilde{N}]^{-1}\tilde{\Gamma} + 4\tilde{C}^\dagger\tilde{B}^\dagger\right)}{\det\left(\tilde{\Gamma}[A^\dagger - \tilde{Q}A\tilde{N}]^{-1}\tilde{\Gamma}\right)} - 1 \\
&= \det\left(I_{\bar{n}} + 4Z_\ominus^{-1}C(t)^\dagger B^\dagger N^{-1}e^{2sA}\right) - 1 \qquad (5.3a) \\
&= \det\left(I_{\bar{n}} + 4Z_\oplus^{-1}e^{-2sA^\dagger}C(t)^\dagger B^\dagger N^{-1}\right) - 1\,, \qquad (5.3b)
\end{aligned}
$$

where

$$
\begin{aligned}
Z_\ominus &= \left(e^{2sA^\dagger}N^{-1}e^{2sA} + Q(t)\right)\left[A^\dagger e^{2sA^\dagger}N^{-1}e^{2sA} - Q(t)A\right]^{-1} \\
&\quad\times\left(e^{2sA^\dagger}N^{-1}e^{2sA} + Q(t)\right)\,, \qquad (5.4a) \\
Z_\oplus &= \left(N^{-1} + e^{-2sA^\dagger}Q(t)e^{-2sA}\right)\left[A^\dagger N^{-1} - e^{-2sA^\dagger}Q(t)e^{-2sA}A\right]^{-1} \\
&\quad\times\left(N^{-1} + e^{-2sA^\dagger}Q(t)e^{-2sA}\right)\,. \qquad (5.4b)
\end{aligned}
$$

It is clear that expression (5.3a) with (5.4a) is convenient for evaluating $\frac{\partial}{\partial s}u(s,t)$ when $s \le 0$, whereas (5.3b) with (5.4b) is convenient for evaluating numerically $\frac{\partial}{\partial s}u(s,t)$ when $s \ge 0$.

Finally, for the time derivative, we have

$$\begin{aligned}\frac{\partial}{\partial t}u(s,t) &= 8\tilde{B}^\dagger\tilde{\Gamma}^{-1}\left[\left(A^\dagger\right)^2+\tilde{Q}A^2\tilde{N}\right]\tilde{\Gamma}^{-1}\tilde{C}^\dagger\\ &= \frac{\det\left(\tilde{\Gamma}\left[\left(A^\dagger\right)^2+\tilde{Q}A^2\tilde{N}\right]^{-1}\tilde{\Gamma}+8\tilde{C}^\dagger\tilde{B}^\dagger\right)}{\det\left(\tilde{\Gamma}\left[\left(A^\dagger\right)^2+\tilde{Q}A^2\tilde{N}\right]^{-1}\tilde{\Gamma}\right)}-1\\ &= \det\left(I_{\bar{n}}+8\,W_\ominus^{-1}C(t)^\dagger B^\dagger N^{-1}e^{2sA}\right)-1 \qquad (5.5a)\\ &= \det\left(I_{\bar{n}}+8\,W_\oplus^{-1}e^{-2sA^\dagger}C(t)^\dagger B^\dagger N^{-1}\right)-1\,, \qquad (5.5b)\end{aligned}$$

where

$$\begin{aligned}W_\ominus &= \left(e^{2sA^\dagger}N^{-1}e^{2sA}+Q(t)\right)\left[\left(A^\dagger\right)^2e^{2sA^\dagger}N^{-1}e^{2sA}+Q(t)A^2\right]^{-1}\\ &\quad\times\left(e^{2sA^\dagger}N^{-1}e^{2sA}+Q(t)\right), \qquad (5.6a)\\ W_\oplus &= \left(N^{-1}+e^{-2sA^\dagger}Q(t)e^{-2sA}\right)\left[\left(A^\dagger\right)^2N^{-1}+e^{-2sA^\dagger}Q(t)e^{-2sA}A^2\right]^{-1}\\ &\quad\times\left(N^{-1}+e^{-2sA^\dagger}Q(t)e^{-2sA}\right). \qquad (5.6b)\end{aligned}$$

Again, it is clear that expression (5.5a) with (5.6a) is convenient for evaluating $\frac{\partial}{\partial t}u(s,t)$ when $s\le 0$, whereas (5.5b) with (5.6b) is convenient for evaluating numerically $\frac{\partial}{\partial t}u(s,t)$ when $s\ge 0$.

5.2. **Appendix: Alternative formulations of the solution of HF and its space and time derivatives.** The functions $L_1(s,t)$ and $L_2(s,t)$ in formula (3.19) can be rewritten as

$$\begin{aligned}L_1(s,t) &= -\tilde{C}\tilde{N}\tilde{\Gamma}^{-1}A^{\dagger^{-1}}\tilde{C}^\dagger = \frac{\det\left(I_{\bar{n}}-(A^\dagger)^{-1}\tilde{Q}A\tilde{N}\right)}{\det(\tilde{\Gamma})}-1\\ &= \frac{\det\left(e^{2sA^\dagger}N^{-1}e^{2sA}-(A^\dagger)^{-1}Q(t)A\right)}{\det\left(e^{2sA^\dagger}N^{-1}e^{2sA}+Q(t)\right)}-1 \qquad (5.7a)\\ &= \frac{\det\left(N^{-1}-(A^\dagger)^{-1}e^{-2sA^\dagger}Q(t)e^{-2sA}A\right)}{\det\left(N^{-1}+e^{-2sA^\dagger}Q(t)e^{-2sA}\right)}-1\,, \qquad (5.7b)\\ L_2(s,t) &= \tilde{B}\tilde{\Gamma}^{-1}A^{\dagger^{-1}}\tilde{C}^\dagger = \frac{\det(\tilde{\Gamma}+\left(A^\dagger\right)^{-1}\tilde{C}^\dagger\tilde{B}^\dagger)}{\det(\tilde{\Gamma})}-1\\ &= \frac{\det\left(e^{2sA^\dagger}N^{-1}e^{2sA}+Q(t)+(A^\dagger)^{-1}C(t)^\dagger B^\dagger N^{-1}e^{2sA}\right)}{\det\left(e^{2sA^\dagger}N^{-1}e^{2sA}+Q(t)\right)}-1 \qquad (5.7c)\\ &= \frac{\det\left(N^{-1}+e^{-2sA^\dagger}Q(t)e^{-2sA}+e^{-2sA^\dagger}(A^\dagger)^{-1}C(t)^\dagger B^\dagger N^{-1}\right)}{\det\left(N^{-1}+e^{-2sA^\dagger}Q(t)e^{-2sA}\right)}-1\,, \qquad (5.7d)\end{aligned}$$

where expressions (5.7a) and (5.7c) are convenient for evaluating numerically $\mathbf{m}(s,t)$ when $s\le 0$, whereas expressions (5.7b) and (5.7d) are convenient for evaluating numerically $\mathbf{m}(s,t)$ when $s\ge 0$.

Similarly, for the space derivative we have

$$\frac{\partial}{\partial s}\left(m_1 + i\, m_2\right) = -2\Big(\frac{\partial}{\partial s}L_1\Big)L_2 - 2(1+L_1)\Big(\frac{\partial}{\partial s}L_2\Big)\,, \tag{5.8a}$$

$$\frac{\partial}{\partial s}m_3 = 4\,\mathrm{Re}\left[\Big(\frac{\partial}{\partial s}L_1\Big)(1+L_2^*)\right], \tag{5.8b}$$

with

$$\begin{aligned}\frac{\partial}{\partial s}L_1 &= 2\tilde{C}A\tilde{N}\tilde{\Gamma}^{-1}{A^\dagger}^{-1}\tilde{C}^\dagger + 2\tilde{C}\tilde{N}\tilde{\Gamma}^{-1}[A^\dagger - \tilde{Q}A\tilde{N}]\tilde{\Gamma}^{-1}{A^\dagger}^{-1}\tilde{C}^\dagger\\ &= \frac{\det\left(e^{2sA^\dagger}N^{-1}e^{2sA} + Q(t) + 2\big(A^\dagger\big)^{-1}C^\dagger(t)C(t)A\right)}{\det\left(e^{2sA^\dagger}N^{-1}e^{2sA} + Q(t)\right)}\\ &\quad - \det\left(I_{\bar{n}} - 2\,Z_\ominus^{-1}(A^\dagger)^{-1}C^\dagger(t)C(t)\right) \qquad (5.9a)\\ &= \frac{\det\left(N^{-1} + e^{-2sA^\dagger}Q(t)e^{-2sA} + 2(A^\dagger)^{-1}e^{-2sA^\dagger}C^\dagger(t)C(t)e^{-2sA}A\right)}{\det\left(N^{-1} + e^{-2sA^\dagger}Q(t)e^{-2sA}\right)}\\ &\quad - \det\left(I_{\bar{n}} - 2\,Z_\oplus^{-1}(A^\dagger)^{-1}e^{-2sA^\dagger}C^\dagger(t)C(t)e^{-2sA}\right), \qquad (5.9b)\end{aligned}$$

and

$$\begin{aligned}\frac{\partial}{\partial s}L_2(s,t) &= -2\tilde{B}^\dagger\tilde{\Gamma}^{-1}[A^\dagger - \tilde{Q}A\tilde{N}]\tilde{\Gamma}^{-1}{A^\dagger}^{-1}\tilde{C}^\dagger\\ &= \det\left(I_{\bar{n}} - 2\,Z_\ominus^{-1}(A^\dagger)^{-1}C(t)^\dagger B^\dagger N^{-1}e^{2sA}\right) - 1 \qquad (5.9c)\\ &= \det\left(I_{\bar{n}} - 2\,Z_\oplus^{-1}e^{-2sA^\dagger}(A^\dagger)^{-1}C(t)^\dagger B^\dagger N^{-1}\right) - 1\,, \qquad (5.9d)\end{aligned}$$

where $Z_\ominus$ and $Z_\oplus$ are defined as in (5.4). It is clear that expressions (5.9a) and (5.9c) with (5.4a) are convenient for evaluating $\frac{\partial}{\partial s}\mathbf{m}(s,t)$ when $s \le 0$, whereas expressions (5.9a) and (5.9c) with (5.4b) are convenient for evaluating numerically $\frac{\partial}{\partial s}\mathbf{m}(s,t)$ when $s \ge 0$.

Analogously, for the time derivative we have

$$\frac{\partial}{\partial t}\left(m_1 + i\, m_2\right) = -2\big(\frac{\partial}{\partial t}L_1\big)L_2 - 2(1+L_1)\big(\frac{\partial}{\partial t}L_2\big)\,, \tag{5.10a}$$

$$\frac{\partial}{\partial t}m_3 = 4\,\mathrm{Re}\left[\big(\frac{\partial}{\partial t}L_1\big)(1+L_2^*)\right], \tag{5.10b}$$

with

$$\begin{aligned}\frac{\partial}{\partial t}L_1 &= 4i\tilde{C}A^2\tilde{N}\tilde{\Gamma}^{-1}{A^\dagger}^{-1}\tilde{C}^\dagger - 4i\tilde{C}\tilde{N}\tilde{\Gamma}^{-1}[(A^\dagger)^2 + \tilde{Q}A^2\tilde{N}]\tilde{\Gamma}^{-1}{A^\dagger}^{-1}\tilde{C}^\dagger\\ &= \frac{\det\left(e^{2sA^\dagger}N^{-1}e^{2sA} + Q(t) + 4i\big(A^\dagger\big)^{-1}C^\dagger(t)C(t)A^2\right)}{\det\left(e^{2sA^\dagger}N^{-1}e^{2sA} + Q(t)\right)}\\ &\quad - \det\left(I_{\bar{n}} - 4i\,W_\ominus^{-1}(A^\dagger)^{-1}C^\dagger(t)C(t)\right) \qquad (5.11a)\\ &= \frac{\det\left(N^{-1} + e^{-2sA^\dagger}Q(t)e^{-2sA} + 4i(A^\dagger)^{-1}e^{-2sA^\dagger}C^\dagger(t)C(t)e^{-2sA}A^2\right)}{\det\left(N^{-1} + e^{-2sA^\dagger}Q(t)e^{-2sA}\right)}\\ &\quad - \det\left(I_{\bar{n}} - 4i\,W_\oplus^{-1}(A^\dagger)^{-1}e^{-2sA^\dagger}C^\dagger(t)C(t)e^{-2sA}\right), \qquad (5.11b)\end{aligned}$$

and

$$\frac{\partial}{\partial t}L_2(s,t) = 4i\tilde{B}^\dagger\tilde{\Gamma}^{-1}[(A^\dagger)^2 + \tilde{Q}A\tilde{N}]\tilde{\Gamma}^{-1}{A^\dagger}^{-1}\tilde{C}^\dagger$$

$$= \det\left(I_{\bar{n}} - 4i\, W_{\ominus}^{-1}(A^{\dagger})^{-1}C(t)^{\dagger}B^{\dagger}N^{-1}e^{2sA}\right) - 1 \tag{5.11c}$$

$$= \det\left(I_{\bar{n}} - 4i\, W_{\oplus}^{-1}e^{-2sA^{\dagger}}(A^{\dagger})^{-1}C(t)^{\dagger}B^{\dagger}N^{-1}\right) - 1\,, \tag{5.11d}$$

where $W_{\ominus}$ and $W_{\oplus}$ are defined as in (5.6). It is clear that expressions (5.11a) and (5.11c) with (5.6a) are convenient for evaluating $\frac{\partial}{\partial t}\mathbf{m}(s,t)$ when $s \leq 0$, whereas expressions (5.11a) and (5.11c) with (5.6b) are convenient for evaluating numerically $\frac{\partial}{\partial t}\mathbf{m}(s,t)$ when $s \geq 0$.

Acknowledgements. The authors thanks F. Borghero, A. della Vedova, S. Lombardo, A. Moro, and C. Rogers for interesting discussions and useful suggestions. The work of MS and FD has been carried out in the framework of a London Mathematical Society Scheme 4 (Research in Pairs) grant on "Propagating, localised waves in ferromagnetic nanowires" (Ref No: 41622). The work of FD and GO has been carried out in the framework of a Progetto Giovani 2017 grant on "Studio di modelli di tipo idrodinamico per il ferromagnetismo" ("Study of models of the hydrodynamic type for ferromagnetism") funded by GNFM (Gruppo Nazionale di Fisica Matematica, National Group for Mathematical Physics), INdAM (Istituto Nazionale di Alta Matematica, National Institute for Advanced Mathematics).

References

[1] A. Aharoni; *Introduction to the Theory of Ferromagnetism*, International Series of Monographs in Physics, Oxford University Press, New York, 2000.

[2] M. J. Ablowitz, D. J. Kaup, A. C. Newell, H. Segur; *The Inverse scattering transform. Fourier analysis for nonlinear problems*, Stud. Appl. Math., **53**, 249–315 (1974).

[3] M. J. Ablowitz, B. Prinari, A.D. Trubatch; *Discrete and Continuous Nonlinear Schrödinger Systems*, London Math. Soc. Lecture Notes Series, **302**, Cambridge Univ. Press, Cambridge, 2004.

[4] M. J. Ablowitz, H. Segur; *Solitons and the Inverse Scattering Transform*, SIAM, Philadelphia, 1981.

[5] T. Aktosun, C. van der Mee; *Explicit Solutions to the Korteweg-de Vries Equation on the Half Line*, Inverse Problems, **22**, 2165–2174 (2006).

[6] T. Aktosun, F. Demontis, C. van der Mee; *Exact solutions to the focusing nonlinear Schrödinger equation*, Inverse Problems **23**, 2171–2195 (2007).

[7] T. Aktosun, F. Demontis, C. van der Mee; *Exact solutions to the Sine-Gordon Equation*, Journal of Mathematical Physics, **51**, (2010).

[8] N. Asano, Y. Kato; *Non-self-adjoint Zakharov-Shabat operator with a potential of the finite asymptotic values. I. Direct and inverse scattering problems*, J. Math. Phys., **22**, 2780–2793 (1980).

[9] N. Asano, Y. Kato; *Non-self-adjoint Zakharov-Shabat operator with a potential of the finite asymptotic values. II. Inverse problem*, J. Math. Phys., **25**, 570–588 (1984).

[10] S. D. Bader, S. S. P. Parkin; *Spintronics*, Annu. Rev. Condens. Matter Phys., **1**, 71–88 (2010).

[11] G. Biondini, G. Kovacic; *Inverse scattering transform for the focusing nonlinear Schrödinger equation with nonzero boundary conditions*, J. Math. Phys., **55**, 031506 (2014).

[12] M. Boiti, F. Pempinelli; *The spectral transform for the NLS equation with left-right asymmetric boundary conditions*, Nuovo Cimento A, **69**, 213–227 (1982).

[13] L.D. Bookman, M. A. Hoefer; *Perturbation theory for propagating magnetic droplet solitons*, Proc. R. Soc. A, **471**(2179), 20150042 (2015).

[14] S. Bonetti, V. Tiberkevich, G. Consolo, G. Finocchio, P. Muduli, F. Mancoff, A. Slavin, J. Åkerman; *Experimental evidence of self-localized, and propagating spin wave modes in obliquely magnetized current-driven nanocontacts*, Phys. Rev. Lett., **105**, 217204 (2010).

[15] F. Calogero, *Why Are Certain Nonlinear PDEs Both Widely Applicable and Integrable?*, in V.E. Zakharov (Ed.), *What is Integrabily*, Springer (1991).

[16] F. Calogero, A. Degasperis; *Spectral transforms and solitons*, Amsterdam North-Holland (1982).

[17] R. Y. Chiao, E. Garmire, C. H. Townes; *Self-trapping of optical beams*, Phys. Rev. Lett. 13, 479–482 (1964).

[18] S. Chung, A. Eklund, E. Iacocca, S. M. Mohseni, S. R. Sani, L. Bookman, M. A. Hoefer, R.K. Dumas, J. Åkerman; *Magnetic droplet nucleation boundary in orthogonal spin-torque nano-oscillators*, Nature Comm., **7**, 11209 (2016).

[19] S. Chung, S. M. Mohseni, A. Eklund, P. Dürrenfeld, M. Ranjbar, S. R. Sani, T. N. Anh Nguyen, R. K. Dumas, J. Åkerman; *Magnetic droplet solitons in orthogonal spin valves*, Low Temp. Phys., **41**, 833 (2015).

[20] S. Chung, S. M. Mohseni, S. R. Sani, E. Iacocca, R. K. Dumas, T. N. Anh Nguyen, Ye. Pogoryelov, P. K. Muduli, A. Eklund, M. Hoefer, J. Åkerman; *Spin transfer torque generated magnetic droplet solitons*, J. App. Phys., **115**, 172612 (2014).

[21] L.S. Da Rios, *Sul moto di un liquido indefinito con un filetto vorticoso*, Rend. Circ. Mat. Palermo, 22, 117–135 (1906) [in Italian].

[22] F. Demontis, B. Prinari, C. van der Mee, F. Vitale; *The inverse scattering transform for the defocusing nonlinear Schrödinger equation with nonzero boundary conditions*, Stud. Appl. Math., **131**, 1–40 (2013).

[23] F. Demontis, B. Prinari, C. van der Mee, F. Vitale; *The inverse scattering transform for the focusing nonlinear Schrödinger equation with asymmetric boundary conditions*, J. Math. Phys., **55** 101505 (2014).

[24] F. Demontis, S. Lombardo, M. Sommacal, C. van der Mee, F. Vargiu; *Effective Generation of Closed-form Soliton Solutions of the Continuous Classical Heisenberg Ferromagnet Equation*, Comm. Nonlin. Sc. Num. Sim., **64**, 35–65 (2018).

[25] F. Demontis, *Exact solutions to the modified Korteweg-de Vries equation*, Theoretical and Mathematical Physics, **168** (1), 886–897 (2011).

[26] F. Demontis, G. Ortenzi, C. van der Mee; *Exact Solutions of the Hirota Equation and Vortex Filaments Motion*, Physica D **313**, 61–80 (2015).

[27] F. Demontis, C. van der Mee; *Explicit solutions of the cubic matrix nonlinear Schrödinger equation*, Inverse Problems **24**, 16 pp. (2008).

[28] B. Dubrovin, T. Grava, C. Klein; *On universality of critical behaviour in the focusing nonlinear Schrödinger equation, elliptic umbilic catastrophe and the tritronquée solution to the Painlevé-I equation*, Journal of Nonlinear Science, **19**(1), 57–94 (2009)

[29] L. D. Faddeev, and L. A. Takhtajan; *Hamiltonian methods in the theory of solitons*, Springer, Berlin and New York, 1987.

[30] H. C. Fogedby; *Solitons and magnons in the classical Heisenberg chain*, J. Phys. A: Math. Gen., 13, 14671499 (1980).

[31] M. Gage, R.S. Hamilton; *The heat equation shrinking convex plane curves*, J. Differential Geom., 23, no. 1, 69–96 (1986).

[32] J. Garnier, K. Kalimeris; *Inverse scattering perturbation theory for the nonlinear Schrödinger equation with non-vanishing background*, J. Phys. A: Math. Theor., **45**, 035202 (2012).

[33] V. S. Gerdjikov, P. P. Kulish; *Completely integrable Hamiltonian systems connected with a nonselfadjoint Dirac operator*, Bulgar. J. Phys., **5**(4), 337–348 (1978) [in Russian].

[34] S. Gutiérrez, A. de Laire; *Self-similar solutions of the one-dimensional Landau-Lifshitz-Gilbert equation*, Nonlinearity, **28**(5), 1307-1350 (2015).

[35] A. Hasegawa, F. Tappert; *Transmission of stationary nonlinear optical pulses in dispersive dielectric fibers. I. Anomalous dispersion*, App. Phys. Lett., **23**(3) 142–144 (1973).

[36] A. Hasegawa, F. Tappert; *Transmission of stationary nonlinear optical pulses in dispersive dielectric fibers. II. Normal dispersion*, App. Phys. Lett., **23**(3) 171–172 (1973).

[37] H. Hasimoto, *Soliton on a vortex filament*, J. Fluid. Mech. **51** 477–485 (1972).

[38] M. A. Hoefer, T. Silva, M. Keller; *Theory for a dissipative droplet soliton excited by a spin torque nanocontact*, Phys. Rev. B **82**(5), 054432 (2010).

[39] M. A. Hoefer, M. Sommacal; *Propagating two-dimensional magnetic droplets*, Physica D **241**, 890–901 (2012).

[40] M.A. Hoefer, M. Sommacal, T. Silva; *Propagation, and control of nano-scale, magnetic droplet solitons*, Phys. Rev. B **85**(21), 214433 (2012).

[41] E. Iacocca, R. K. Dumas, L. Bookman, M. Mohseni, S. Chung, M. A. Hoefer, J. Åkerman; *Confined dissipative droplet solitons in spin-valve nanowires with perpendicular magnetic anisotropy*, Phys. Rev. Lett. **112**, 047201 (2014).

[42] E. Iacocca, T.J. Silva, M.A. Hoefer, *Breaking of Galilean invariance in the hydrodynamic formulation of ferromagnetic thin films*, Phys. Rev. Lett. **118**, 017203 (2017).
[43] B. Ivanov, A. Kosevich, *Bound-states of a large number of magnons in a ferromagnet with one-ion anisotropy*, Zh. Eksp. Teor. Fiz. **72**(5), 2000–2015 (1977).
[44] B. A. Ivanov, and V. A. Stephanovich; *Two-dimensional soliton dynamics in ferromagnets*, Phys. Lett. A **141**(1), 89–94 (1989).
[45] B. A. Ivanov, C. E. Zaspel, I. A. Yastremsky; *Small-amplitude mobile solitons in the two-dimensional ferromagnet*, Phys. Rev. B **63**(13), 134413 (2001).
[46] T. Kawata, H. Inoue; *Eigenvalue problem with nonvanishing potentials*, J. Phys. Soc. Japan **43**, 361–362 (1977).
[47] T. Kawata, H. Inoue; *Inverse scattering method for the nonlinear evolution equations under nonvanishing conditions*, J. Phys. Soc. Japan, **44**, 1722–1729 (1978).
[48] B. G. Konopelchenko, G. Ortenzi, *Quasi-classical approximation in vortex filament dynamics. Integrable systems, gradient catastrophe and flutter*, Studies in Applied Mathematics, 130(2) , 167–199 (2013).
[49] A. Kosevich, B. Ivanov, A. Kovalev; *Magnetic solitons*, Phys. Rep., **194**(3–4), 117–238 (1990).
[50] P. P. Kulish, S. V. Manakov, a L. D. Faddeev; *Comparison of the exact quantum and quasiclassical results for a nonlinear Schrödinger equation*, Theor. Math. Phys. **28**, 615–620 (1976).
[51] M. Lakshmanan, K. Porsezian, M. Daniel; *Effect of discreteness on the continuum limit of the Heisenberg spin chain*, Phys. Lett. A **139**(9), 483–488 (1988).
[52] M. Lakshmanan, T. W. Ruijgrok, C. J. Thompson; *On the dynamics of a continuum spin system*, Physica A **84**(3), 577-590 (1976).
[53] M. Lakshmanan, *Continuum spin system as an exactly solvable dynamical system*, Phys. Lett., **61A**, 53–54 (1977).
[54] G. Lamb, Jr., *Solitons and the Motion of Helical Curves*, Phys. Rev. Lett., **37**, 235 (1976).
[55] J. Langer, R. Perline; *The Hasimoto transformation and integrable flows on curves*, Applied Mathematics Letters **3**(2), 61–64 (1990).
[56] J. Langer, R. Perline; *Poisson Geometry of the Filament Equation*, J. Nonlin. Sci., **3**, 71–93 (1991).
[57] J. Lau, J. Shaw; *Magnetic nanostructures for advanced technologies: fabrication, metrology, and challenges*, J. Phys. D: Appl. Phys., **44**, 303001 (2011).
[58] J. Leon; *The Dirac inverse spectral transform: kinks and boomerons*, J. Math. Phys., **21**(10), 2572–2578 (1980).
[59] T. Levi-Civita, E. Amaldi; *Lezioni di Meccanica Razionale*, Vol. 1, Zanichelli Editore, (1974, first edition 1923).
[60] F. Maciá, D. Backes, A.D. Kent; *Stable magnetic droplet solitons in spin-transfer nanocontacts*, Nat. Nano. **9**, 992–996 (2014).
[61] M. D. Maiden, L. D. Bookman, M. A. Hoefer; *Attraction, merger, reflection,, and annihilation in magnetic droplet soliton scattering*, Phys. Rev. B, **89**(18), 180409 (2014).
[62] S. M. Mohseni, S. R. Sani, J. Persson, T. N. Anh Nguyen, S. Chung, Ye. Pogoryelov, P. K. Muduli, E. Iacocca, A. Eklund, R. K. Dumas, S. Bonetti, A. Deac, M. A. Hoefer, J. Åkerman; *Spin torque-generated magnetic droplet solitons*, Science, **339**, 1295–1298 (2013).
[63] S. M. Mohseni, S. R. Sani, R. K. Dumas, J. Persson, T. N. Anh Nguyen, S. Chung, Ye. Pogoryelov, P. K. Muduli, E. Iacocca, A. Eklund, J. Åkerman; *Magnetic droplet solitons in orthogonal nano-contact spin torque oscillators*, Physica B, **435**, 84–87 (2014).
[64] K. Nakamura, T. Sasada, *Soliton and wave trains in ferromagnets*, Phys. Lett. A, **48A**(9), 321–322 (1974).
[65] K. Nakamura, T. Sasada, *Gauge equivalence between one-dimensional Heisenberg ferromagnets with single-site anisotropy and nonlinear Schrodinger equations*, J. Phys. C: Solid State Phys., **15**, 915–918, (1982).
[66] K. Nakayama, H. Segur, M. Wadati; *Integrability and the motion of curves*, Phys. Rev. Lett. 69, 18, 2603 (1992).
[67] S. P. Novikov, S. V. Manakov, L. B. Pitaevskii, V.E. Zakharov; *Theory of Solitons. The Inverse Scattering Method*, Plenum Press, New York, 1984.
[68] Y.-C. Ma, *The perturbed plane-wave solutions of the cubic Schrödinger equation*, Stud. Appl. Math., **60**, 43–58 (1979).

[69] N. Papanicolaou, T.N. Tomaras, *Dynamics of Magnetic Vortices*, Nucl. Phys. B, **360**, 425–462 (1991).
[70] C. Rogers, W. K. Schief; *Intrinsic Geometry of the NLS Equation and its Auto-Bäcklund Transformation*, Stud. Appl. Math., **101**, 267–287 (1998).
[71] W. K. Schief, C. Rogers; *Binormal Motion of Curves of Constant Curvature and Torsion. Generation of Soliton Surfaces*, Proc. Roy. Soc. Lond. A, **455**, 3163–3188 (1999).
[72] C. Rogers, W. K. Schief; *On Geodesic Hydrodynamic Motions. Heisenberg Spin Connections*, J. Math. Anal. Appl., **251**, 855–870 (2000).
[73] C. Rogers, *On the Geometry of Spatial Hydrodynamic Motions. Solitonic Connections*, in R. Monaco (Ed.), *Proceedings XIth International Conference on Waves and Stability in Continuous Media*, 458–470 (2002).
[74] C.Rogers, W. K. Schief; *Novel integrable reductions in nonlinear continuum mechanics via geometric constraints*, J. Math. Phys. **44**, 3341–3369 (2003).
[75] C. J. Pethick, H. Smith; *Bose-Einstein Condensation in Dilute Gases*, Cambridge University Press (2002).
[76] B. Piette, W. J. Zakrzewski; *Localized solutions in a two-dimensional Landau-Lifshitz model*, Physica D **119**(3), 314–326 (1998).
[77] P. G. Saffman; *Vortex Dynamics*, Cambridge University Press UK (1992).
[78] M. Sparks, *Ferromagnetic relaxation theory*, McGraw-Hill (1965).
[79] V. I. Talanov, *About self-focusing of light in cubic media*, JETP Lett. 2, 138–142 (1965).
[80] V. I. Talanov, *On self-focusing of the wave beams in nonlinear media*, JETP Lett. 11, 199–201 (1970).
[81] L. A. Takhtajan, *Integration of the continuous Heisenberg spin chain through the inverse scattering method*, Phys. Lett., **64A**, 235–237 (1977).
[82] J. Tjon J. Wright; *Solitons in the continuous Heisenberg spin chain*, Phys. Rev. B, **15**, 3470–3476 (1977).
[83] L. A. Turski; *Hydrodynamical description of the continuous Heisenberg chain*, Can. J. Phys., **59**, 511–514 (1981)
[84] C. van der Mee; *Nonlinear evolution models of integrable type*, SIMAI e-Lectures Notes **11** (2013).
[85] C. E. Weatherburn; *Differential Geometry Of Three Dimensions-Vol I*, Cambridge University Press, London (1955).
[86] V. E. Zakharov, A. B. Shabat; *Exact theory of two-dimensional self-focusing and one dimensional self-modulation of waves in nonlinear media*, Sov. Phys. JETP, 34, 62–69 (1972).
[87] V. E. Zakharov, *Hamilton formalism for hydrodynamic plasma models*, Sov Phys. JETP **33**, 927–932 (1971); translated from Ž. Èksper. Teoret. Fiz., **60**, 1714–1726 (1971) [in Russian].
[88] V. E. Zakharov, L. A. Takhtajan; *Equivalence of the nonlinear Schrödinger equation and the equation of a Heisenberg ferromagnet*, Theor. Math. Phys., **38**, 17–23 (1979).

Francesco Demontis
Dipartimento di Matematica e Informatica, Universitá di Cagliari, 09124 Cagliari, Italy
E-mail address: fdemontis@unica.it

Giovanni Ortenzi
Dipartimento di Matematica Pura e Applicazioni, Universitá di Milano Bicocca, 20125 Milano, Italy
E-mail address: giovanni.ortenzi@unimib.it

Matteo Sommacal
Department of Mathematics, Physics and Electrical Engineering, Northumbria University, Newcastle upon Tyne, NE1 8ST, UK
E-mail address: matteo.sommacal@northumbria.ac.uk